NAVAL POSTGRADUATE SCHOOL
Monterey, California

DISSERTATION

SIMULATION OF THE DYNAMIC BEHAVIOR OF EXPLOSION GAS BUBBLES IN A COMPRESSIBLE FLUID MEDIUM

by

James E. Chisum

December, 1996

Thesis Advisor: Young S. Shin

Approved for public release; distribution is unlimited.

REPORT DOCUMENTATION PAGE

Form Approved OMB No. 0704-0188

1. AGENCY USE ONLY (Leave blank)	2. REPORT DATE December 1996	3. REPORT TYPE AND DATES COVERED Doctoral Dissertation

4. TITLE AND SUBTITLE SIMULATION OF THE DYNAMIC BEHAVIOR OF EXPLOSION GAS BUBBLES IN A COMPRESSIBLE FLUID MEDIUM

5. FUNDING NUMBERS

6. AUTHOR(S) Chisum, James E.

7. PERFORMING ORGANIZATION NAME(S) AND ADDRESS(ES)
Naval Postgraduate School
Monterey CA 93943-5000

8. PERFORMING ORGANIZATION REPORT NUMBER

9. SPONSORING/MONITORING AGENCY NAME(S) AND ADDRESS(ES)

10. SPONSORING/MONITORING AGENCY REPORT NUMBER

11. SUPPLEMENTARY NOTES The views expressed in this thesis are those of the author and do not reflect the official policy or position of the Department of Defense or the U.S. Government.

12a. DISTRIBUTION/AVAILABILITY STATEMENT
Approved for public release; distribution is unlimited.

12b. DISTRIBUTION CODE

13. ABSTRACT (maximum 200 words)

Data from one-dimensional (spherically symmetric) analyses was used to examine the effects of compressibility and gas energy on the dynamic behavior of an explosion gas bubble, by comparing the bubble's behavior with experimental results and with analytical results which neglect these factors. Results from two-dimensional (axially symmetric) analyses were used to investigate the behavior of a deep explosion gas bubble in the vicinity of plane rigid or constant pressure boundaries. Previous analytical research into explosion gas bubbles near such boundaries has primarily led to results of a qualitative nature, owing to a complete breakdown of the assumptions made in the analysis at the critical juncture. In the present investigation, it was found possible to characterize the effect of the boundary surface on both the change in the first oscillation period of the bubble and its location at the end of the first oscillation cycle. For a broad range of bubble - boundary standoff distances, these semi-empirical characterizations have a functional form particularly suitable for extension of the quantitative results of this investigation to other explosive charge types, weights, and depths, as has been done for the Willis formula for the free-field oscillation period of explosion gas bubbles.

14. SUBJECT TERMS Underwater Explosions, Bubbles, Eulerian Analysis, Dynamic Behavior.

15. NUMBER OF PAGES 96

16. PRICE CODE

17. SECURITY CLASSIFICATION OF REPORT	18. SECURITY CLASSIFICATION OF THIS PAGE	19. SECURITY CLASSIFICATION OF ABSTRACT	20. LIMITATION OF ABSTRACT
Unclassified	Unclassified	Unclassified	UL

NSN 7540-01-280-5500 Standard Form 298 (Rev. 2-89)
Prescribed by ANSI Std. 239-18 298-102

Approved for public release; distribution is unlimited

SIMULATION OF THE DYNAMIC BEHAVIOR OF EXPLOSION GAS BUBBLES IN A COMPRESSIBLE FLUID MEDIUM

James E. Chisum
Lieutenant Commander, United States Navy
B.S., Southern Oregon State College, 1982
M.S., Naval Postgraduate School, 1992
Mech. Eng., Naval Postgraduate School, 1992

Submitted in partial fulfillment
of the requirements for the degree of

DOCTOR OF PHILOSOPHY IN MECHANICAL ENGINEERING

from the

NAVAL POSTGRADUATE SCHOOL
Dececember 1996

ABSTRACT

Data from one-dimensional (spherically symmetric) analyses was used to examine the effects of compressibility and gas energy on the dynamic behavior of an explosion gas bubble, by comparing the bubble's behavior with experimental results and with analytical results which neglect these factors. Results from two-dimensional (axially symmetric) analyses were used to investigate the behavior of a deep explosion gas bubble in the vicinity of plane rigid or constant pressure boundaries. Previous analytical research into explosion gas bubbles near such boundaries has primarily led to results of a qualitative nature, owing to a complete breakdown of the assumptions made in the analysis at the critical juncture. In the present investigation, it was found possible to characterize the effect of the boundary surface on both the change in the first oscillation period of the bubble and its location at the end of the first oscillation cycle. For a broad range of bubble - boundary standoff distances, these semi-empirical characterizations have a functional form particularly suitable for extension of the quantitative results of this investigation to other explosive charge types, weights, and depths, as has been done for the Willis formula for the free-field oscillation period of explosion gas bubbles.

TABLE OF CONTENTS

ACKNOWLEDGEMENT

The author would like to express his heartfelt thanks to his Dissertation Supervisor, Professor Young Shin, for his support and encouragement throughout the course of the Doctor Program. The assistance and labors of the other members of the Doctor Committee, Professor Anthony Healey, Associate Professor Young Kwon, Associate Professor Clyde Scandrett, and Associate Professor Steven Baker, is also gratefully acknowledged. Their support has been crucial to the successful completion of this research.

I. INTRODUCTION

The survivability of naval ships and submarines is of supreme importance to those who design, build and sail them. Underwater explosions, created by the detonation of mines or torpedoes near naval vessels, clearly represent a significant threat to that survivability. The capacity of such weapons to cause major damage to naval vessels has been recognized since the beginning of the age of modern naval warfare, and has been the subject of extensive investigation since the earliest years of the Second World War.

One result of the allied experience during the Second World War was the realization that the pressure wave resulting from the pulsation (oscillation) of the bubble of gases produced by the detonation of an explosive material underwater can be as important as the primary shock wave in causing damage to a naval vessel. As Hicks (1970a) has noted, this bubble pulsation is the primary cause of the observed "whipping" of ships, and often has a period near that of the hull girder's fundamental flexural vibration mode.

This will, in the worst case, break the back of the ship. Even in less severe situations, the oscillation of the ship's hull may be significantly increased by the timing of the arrival of the secondary pressure pulse radiated when the bubble collapses to its first minimum volume. This can cause appreciable damage to sensitive internal equipment. Furthermore, the increased use of commercial off-the-shelf (COTS) equipment within modern ships, while fiscally necessary and undoubtedly beneficial in the long run, may increase the damage potential of explosion gas bubble oscillations.

Fundamental analysis shows that low frequency vibration input can significantly

increase the resulting response in certain underdamped system configurations. Equipment not designed to withstand the increased response could easily suffer damage that, depending upon ship design, reduces the war fighting capability of the ship. In an age of over-the-horizon saturation targeting, such a calamity may be as bad as breaking the back of the ship.

A significant investment of manpower and time has been expended in analyzing the phenomena associated with the pulsation of explosion gas bubbles, both during and since the Second World War. However, these studies have, for the most part, relied upon many simplifying assumptions. The validity of some of these assumptions were known beforehand to be very inaccurate during certain phases of an explosion gas bubble's motion. In fact, some of these assumptions are least accurate during the times when key explosion gas bubble phenomena are occurring. Predictions of explosion gas bubble behavior from these studies are therefore more likely to be qualitatively correct than quantitatively accurate. This is an important consideration because ship design decisions are based, in part, upon these predictions.

The next section describes some of the important phenomena associated with underwater explosion gas bubbles. Following this is a synopsis of the more significant research that has been previously conducted into underwater explosion gas bubbles. The third and final section of this introductory chapter discusses the objectives of this present research effort, and presents an overview of the remaining chapters.

A. BUBBLE PHENOMENA

Consider a spherical explosive charge located underwater at a considerable distance from any boundary surface. When this charge is detonated, the explosive material is very

rapidly converted into high pressure gaseous reaction products, and a high pressure shock wave is transmitted to and propagated through the surrounding fluid. About 50% of the initial chemical energy of the explosive is transmitted to the fluid in this initial shock wave (Snay, 1957).

Because this shock wave propagates radially outward, the amplitude of the shock wave decreases with increasing distance from the center of the charge. The fluid behind the shock wave front attains a large outward radial velocity. This causes the pressure at some distance behind the shock wave front to drop below the hydrostatic pressure of the fluid ahead of this wave front.

The pressure in the gas bubble is significantly reduced after emission of the primary shock wave, but is still significantly higher than the hydrostatic pressure in the surrounding fluid. This, in conjunction with the radial outflow of fluid from the vicinity of the bubble, causes the bubble to expand rapidly. This expansion continues for a relatively long time, the pressure in the bubble decreasing as the bubble volume increases. The pressure in the gas bubble eventually falls below hydrostatic pressure, but the expansion persists because of the inertia of the outward flowing fluid (Cole, 1948, p. 8).

Eventually, the fluid immediately surrounding the bubble comes to rest. This, together with the very low pressure in the bubble at this time, causes the bubble to begin contracting. The fluid in the immediate vicinity of the bubble begins flowing inward, accelerating the contraction of the bubble. As the volume of the bubble decreases, its internal pressure increases. The pressure within the gas bubble eventually becomes significantly higher than the hydrostatic pressure of the surrounding fluid, and the contraction of the bubble is reversed

abruptly. The inertia of the surrounding fluid together with the compressibility of the bubble gases and the surrounding fluid "thus provide the necessary conditions for an oscillating system, and the bubble does in fact undergo repeated cycles of expansion and contraction" (Cole, 1948, p. 8).

Figure 1-1 illustrates the bubble radius vs. time behavior typically observed in an underwater explosion. Note that the maximum radius of the bubble decreases during subsequent expansions. This is due, at least in part, to the emission of secondary pressure pulses when the bubble radius is near its minimum values. About 66% of the energy remaining in the gas bubble after emission of the primary shock wave is lost during the first expansion-contraction cycle (Cole, 1948, p. 283). Successive bubble pulses are thus weaker, and generally only the first pulse is of practical significance (Cole, 1948, p. 10).

Figure 1-2 shows a typical pressure vs. time curve at fixed distance from an underwater explosion. Although the peak pressure in the secondary pressure pulse is much less than the peak shock wave pressure, the duration of this pulse is greater. The impulses due to the primary shock wave and the first of the bubble pulses are typically comparable (Cole, 1948, p. 364).

Additional phenomena are observed when an explosion occurs near a boundary surface, such as the surface or bottom of the ocean or a nearby structure. When an explosion occurs near a relatively rigid boundary such as the hull of a naval vessel or a hard ocean bottom, the explosion gas bubble migrates toward the boundary during its contraction. The opposite effect is seen when an explosion occurs near a free surface (Snay, 1957). The shape of migrating gas bubbles has also been seen to be non-spherical, as illustrated in Figure 1-3.

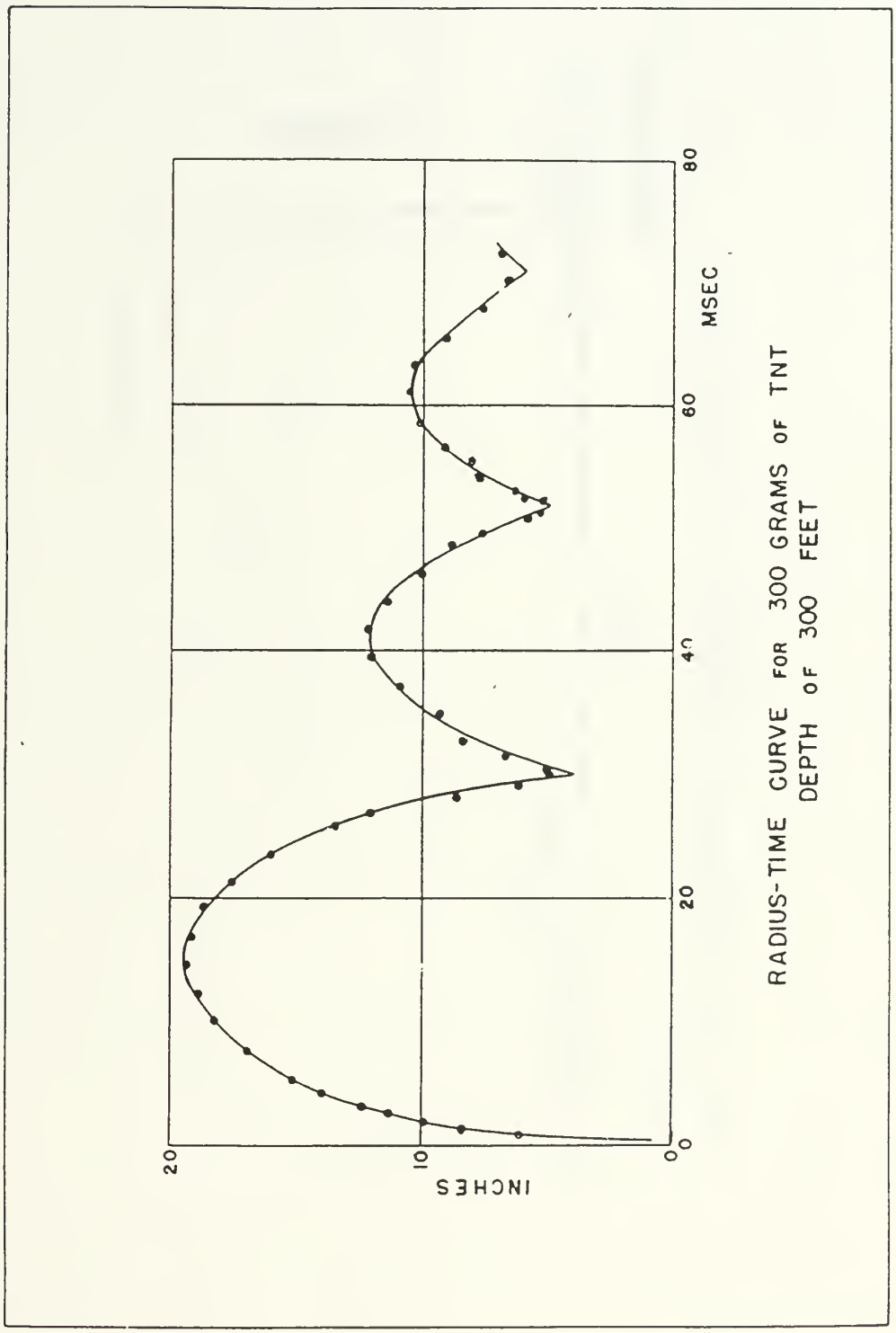

Figure 1-1. Typical Bubble Radius vs. Time Curve [From Swift and Decius (1950)]

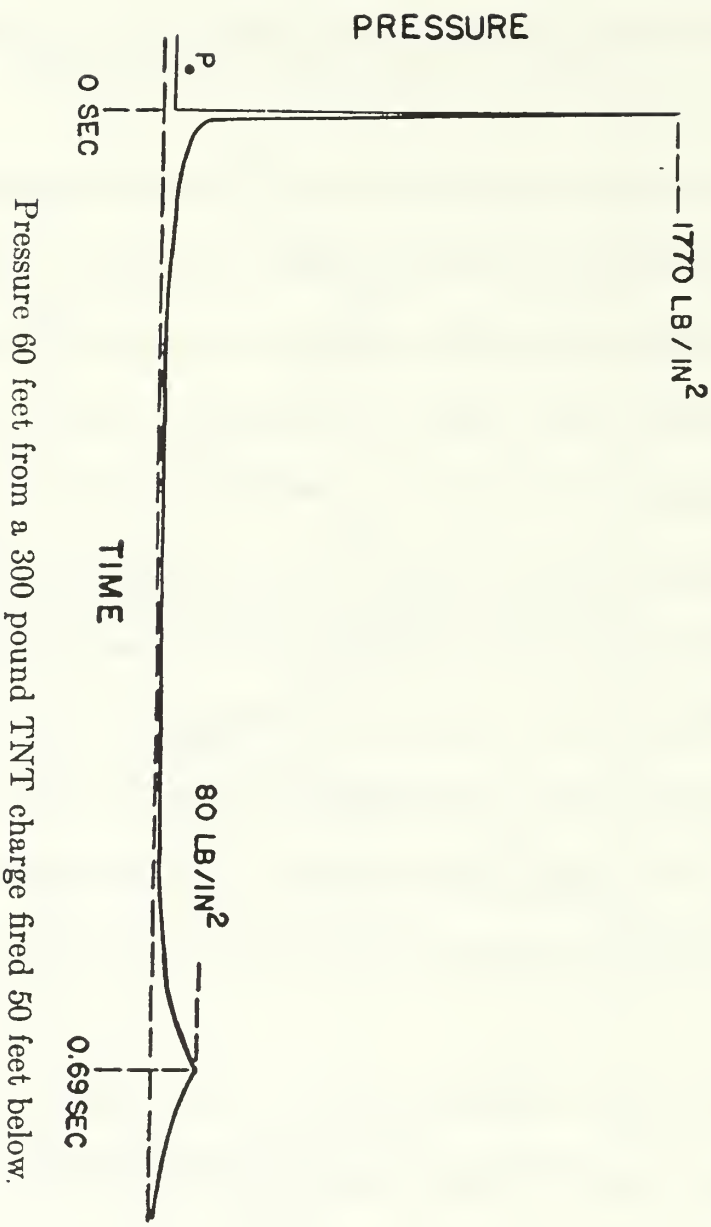

Figure 1-2. Typical Pressure Profile Produced From an Underwater Explosion [From Cole (1948)]

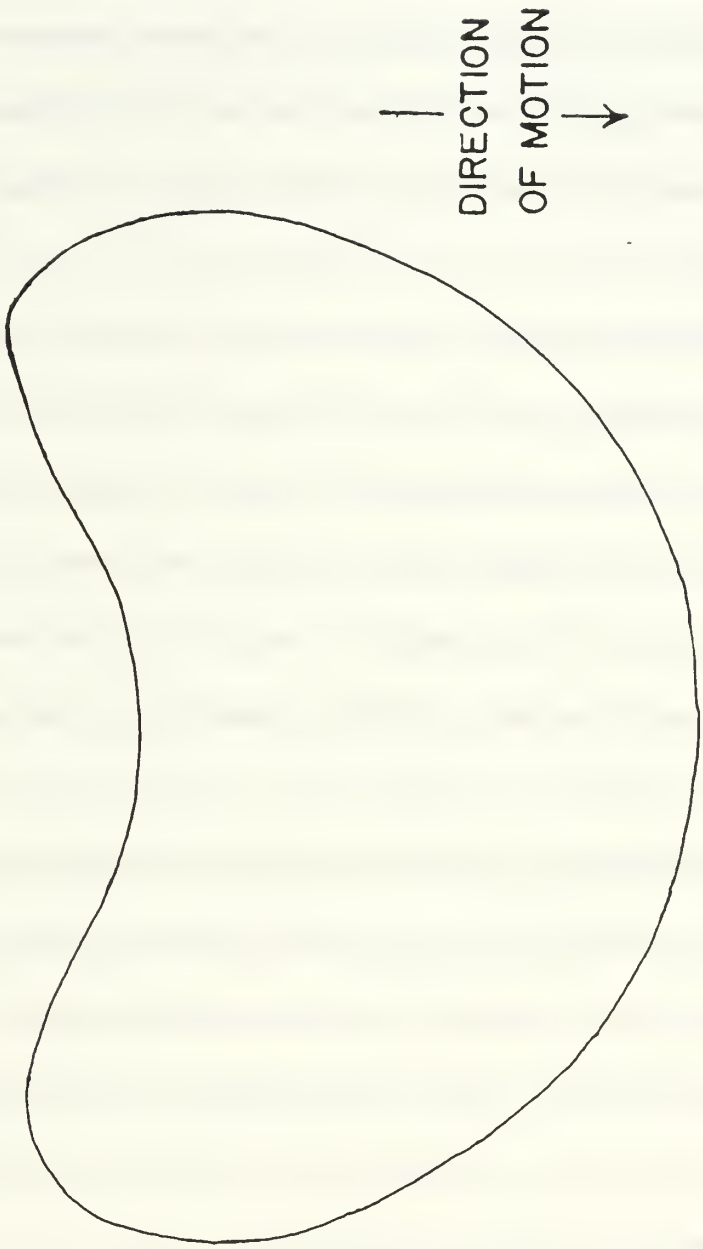

Figure 1-3. Typical Shape for a Migrating Underwater Explosion Gas Bubble [From Cole (1948)]

Since the secondary pressure pulse is emitted when a bubble is near its minimum volume, the migration of a bubble determines where this bubble pulse is emitted from. For an explosion occurring near a naval ship, the migration of the bubble can cause the bubble pulse to occur much closer to the hull, potentially increasing the damage caused to the ship (Hicks, 1970b).

The presence of boundary surfaces also affects the period of the oscillation of the bubble. A rigid boundary causes the period of oscillation of the bubble to increase, and a free surface causes it to decrease (Herring, 1950). Thus, if an explosion occurs near the hull of a ship, the presence of the ship itself can cause the time interval between arrival of the primary shock wave and secondary pressure pulse to become either closer to or further from the fundamental period of the hull girder, significantly affecting the amount of whipping undergone by the ship.

B. PREVIOUS RESEARCH INTO EXPLOSION GAS BUBBLES

Perhaps the earliest contribution related directly to an appreciation and understanding of bubbles was made by Reynolds (1894), who noted the formation of vapor cavitation bubbles in water flowing through a constricted pipe. The first analysis of the dynamic behavior of bubbles was made by Rayleigh (1917), who used conservation of momentum to derive an equation for the collapse of a spherical void.

Lamb (1923) studied the expansion phase of a gas bubble, and derived an expression relating the maximum radius of a bubble to the depth and total energy, neglecting fluid compressibility. Ramsauer (1923) conducted small scale experiments with guncotton which showed reasonably good agreement with Lamb's predicted relationship between maximum

bubble radius and depth. The work of Lamb is the basis for the standard semi-empirical scaling formula for the maximum radius of an explosion gas bubble when buoyancy can be neglected and no boundary surfaces are near the charge. This situation is referred to as the "free-field" case. This scaling formula defines a relationship between the maximum radius of the bubble, the charge weight, and the charge depth. It is termed "semi-empirical" because it depends upon a proportionality constant which varies between different types of explosives, and must be determined through experimentation.

Willis (1941) was the first to succeed in integrating the energy equation for the noncompressive radial motion of free-field explosion gas bubbles, and thereby derive an expression for the period of the first oscillation cycle of the bubble. His work is the basis for the standard semi-empirical formula for the free-field first bubble oscillation period of an explosion gas bubble. This formula defines a scaling relationship for different charge weights and depths, and depends upon an experimentally determined proportionality constant. Willis also conducted experiments to confirm the predicted relationship between charge size, depth, and bubble period, and found good agreement. This result has since been confirmed by other researchers, particularly as to the functional dependency of the first bubble period on the charge depth (Cole, 1948, pp. 280-281).

Herring (1941, 1950) made a number of important contributions to the current understanding of explosion gas bubble phenomena. He predicted, based upon an approximate theoretical development, that one of the effects of fluid compressibility would be to make the bubble radius versus time curve for a free-field bubble asymmetrical, with the contraction being slower the expansion. He conducted an analysis indicating that the radiation of energy,

if fluid compressibility was allowed for, would be negligible when the bubble is large, but that an appreciable radiation of energy could take place at the first bubble minimum.

Herring's most important contribution was the advancement of an approximate theory to account for the effect of simple rigid boundaries or free surfaces (constant pressure boundaries) on explosion gas bubbles during the first oscillation cycle. In this theory, the effects of the boundary surface are treated as small perturbations of the motion of the gas bubble in the absence of the boundary. The boundary is assumed to be remote enough so that the standoff distance to the boundary is large compared to the maximum radius of the bubble, which is assumed to remain nearly spherical. This theory is thus only potentially valid when the boundary surface is fairly remote from the gas bubble. Furthermore, the theory neglects fluid compressibility entirely.

One of the effects of fluid compressibility is a finite wave speed in the fluid; in an incompressible fluid, the wave velocity is infinite. Thus in a compressible fluid there is a finite distance beyond which the presence of a boundary cannot affect an explosion gas bubble during the first oscillation cycle, because even the primary shock wave resulting from detonation of the charge will not have reached the boundary by the end of the first cycle. The theory developed by Herring to account for simple boundary surfaces therefore cannot be correct at large standoff distances, as it assumes an incompressible fluid.

Although Herring's theory for predicting the effect of these simple types of boundary surfaces is still in use, e.g. in the computer code MSWHIP (Hicks, 1971) (which is still being used by the United States Navy to predict the response of naval vessels to underwater explosion gas bubbles), the above discussion begs an answer to the question of when it is

valid. It was never intended to be accurate at small standoff distances, and because it neglects fluid compressibility, it is not valid at large standoff distances.

Another important contribution to the current understanding of explosion gas bubble phenomena was made by Taylor (1943), who derived an expression for the vertical migration of a spherically symmetric bubble due to gravity (buoyancy) in the absence of nearby boundary surfaces, neglecting fluid compressibility. In addition to neglecting fluid compressibility, Taylor's theory is based upon the assumption that artificial forces, which do no work, act to keep the gas bubble spherical. Actual experimental results typically show significant bubble shape departure from spherical, as illustrated in Figure 1-3. In the present application of Taylor's theory for the effects of buoyancy on explosion gas bubbles, use is also made of Herring's theory for the effect of the free surface (if a free surface is not nearby, the bubble is generally deep enough so that buoyancy is not significant).

It is perhaps then not surprising that predictions of explosion gas bubble behavior from the combined Herring-Taylor theory do not agree very well with experimental results. For example, an experimental measurement by Bryant (1950) near a free surface showed a peak bubble migration velocity of 180 ft/s (55 m/s), as compared to a calculated value of 890 ft/s (271 m/s).

Numerous researchers have conducted underwater explosion experiments. Notable among these is Swift and Decius (1950), who conducted a series of experiments to determine relatively accurate values for the proportionality constants in the semi-empirical formulas for the free-field maximum bubble radius and first bubble period, for various types of explosives.

Chertock (1952) developed an approximate method to calculate the bubble pulse

induced whipping response of naval ships and submarines, for explosions occurring very remote from the hull. Hicks (1970a, 1970b, 1971) determined that Chertock's methodology might be applied at smaller standoff distances with simple modifications, and then further modified this procedure to account for bubble migration, using the Herring-Taylor theory. In an attempt to account for the known problems with this theory, his procedure introduces an artificially large drag coefficient, the value of which he has chosen based upon very limited experimental data. This is justified as being "the best [solution] available until fresh experimental results (particularly for the near field) or a more rational theory become available" (Hicks, 1970b). The computer code developed by Hicks, MSWHIP, thus far appears to generally give reasonably accurate results for distant charges; the validity of its predictions at short and intermediate standoff distances is still largely unknown.

Some recent efforts have examined methods to study underwater explosion gas bubble phenomena under laboratory conditions. Schmidt et. al (1987) have studied the problem of conducting very small scale explosive testing (charge weights of about 0.2 g) while maintaining complete similarity, by using a centrifuge to obtain gravitational accelerations of up to 500 times the standard terrestrial gravitational acceleration. Chahine et. al. (1995) have developed a procedure for generating plasma bubbles using a very high energy spark and scaling these plasma bubbles to represent explosion gas bubbles.

As can be seen from the brief summary of previous work given above, much of the current understanding and theoretical development regarding underwater explosions was a result of allied research efforts during the Second World War. Many of the more important papers from this era can be found in the three volume work *Underwater Explosion Research:*

A Compendium of British and American Reports (Office of Naval Research, 1950). A comprehensive summary of the research from this period is provided by Cole (1948).

C. OBJECTIVES OF CURRENT RESEARCH

The above synopsis of previous research into explosion gas bubble phenomena points out several areas in which the existing understanding of these phenomena is inadequate. The existing theoretical understanding of the dynamic behavior of explosion gas bubbles is based upon neglecting fluid compressibility entirely. Only limited, qualitative estimates of what the affects of fluid compressibility might be have been made. And in addition to neglecting fluid compressibility, the existing theory describing the dynamic behavior of explosion gas bubbles near simple rigid or constant pressure boundary surfaces does not cover the situation in which the bubble is fairly close to the boundary. Even for the case in which the bubble is not too close to the boundary surface, the dynamic behavior of the bubble predicted using the existing theory is known to be more qualitatively correct than quantitatively accurate.

The research described in this study was undertaken to rectify some of these shortcomings in the current understanding of explosion gas bubble phenomena. It was believed that, by using a modern numerical analysis computer program based upon a finite control volume (Eulerian) method, it would be possible to quantitatively investigate explosion gas bubble phenomena which had heretofore been understood only qualitatively.

The first goal of this study was to examine the feasibility of using a finite control volume numerical analysis technique to investigate underwater explosion phenomena, and if this method proved serviceable, to investigate the effects of fluid compressibility and internal gas energy on the dynamic behavior of explosion gas bubbles. The second objective was to

investigate the effects of plane rigid and constant pressure boundaries on important aspects of the dynamic behavior of explosion gas bubbles, including fluid compressibility and internal energy, and to quantitatively characterize these effects.

Two specific aspects of the dynamic behavior of bubbles near boundaries were investigated. The first of these was the change in the period of the bubble caused by the boundary. The bubble period is important because the time interval between arrival of the primary shock wave and the first bubble pulse can be very near the fundamental bending mode period of a ship's hull girder. Thus, if the boundary causes this time interval to become even closer to this hull girder bending mode period, the resultant whipping can be increased due to resonance. As discussed earlier, the impulses due to the primary shock wave and the first bubble pulse are comparable in magnitude, while the impulses from subsequent bubble pulses are much smaller. The other aspect of a bubble's dynamic behavior that was investigated was the migration of the bubble at the end of the first expansion-contraction cycle, either towards or away from the boundary. Because pressures fall off with increasing distance, it is important to know where the bubble is located when the first bubble pulse is emitted.

The numerical analysis approach used for this research is described in the next chapter. Chapter III describes the application of this analysis approach to an investigation of the affects of fluid compressibility and internal gas energy on a free-field explosion gas bubble, and compares results from this analysis approach with both experimental and analytical results. The effects of rigid and constant pressure boundaries on explosion gas bubbles, including fluid compressibility and internal gas energy, are examined in Chapter IV. Chapter V then summarizes the results from this study.

This dissertation illustrates the application of a finite volume based numerical analysis technique for investigation of underwater explosion gas bubbles. This technique was used to investigate the effects of fluid compressibility and internal energy on a free-field explosion gas bubble. This analysis procedure was also used to quantitatively characterize the effects of rigid and constant pressure boundaries on explosion gas bubbles, when internal energy and fluid compressibility are not neglected. The quantitative characterizations derived have a form suitable for use in scaling these results for other explosive charge types, weights, and depths.

II. NUMERICAL SOLUTION TECHNIQUE

Because underwater explosions involve the flow of liquids and gases, and a high pressure shock wave, numerical analysis of underwater explosion phenomena in the region near the charge using standard Lagrangian based finite element programs is not practical. In a Lagrangian based finite element program, the elements deform in response to the pressure on the faces of the element. This leads to elements in the region of the shock front being severely deformed (crushed), and the time step size per iteration becoming very small, so that the solution advances very slowly in time.

The numerical analyses described in this study were therefore conducted using an Eulerian based finite volume program. The computer program MSC/DYTRAN (The MacNeal Schwendler Corporation, 1995) was used for the numerical analyses conducted during this investigation. The analyses used the multi-material Eulerian processor in this program, which is based upon the computer program MSC/PISCES (The MacNeal Schwendler Corporation, 1991). This processor provides the flexibility of general connectivity for Eulerian finite volumes, so the finite volumes are not restricted as to shape. This feature is useful when a large volume of fluid must be discretized, but the area of interest is relatively small. Other Eulerian based programs typically require a uniform discretization, which, for analysis of an underwater explosion gas bubble, would require either an unacceptably coarse mesh or an unacceptably large number of finite volumes. This program also provides a constitutive equation suitable for modeling of explosive charge detonation, and a detonation wave front algorithm for detonating an explosive material.

This processor uses the control volume method to solve the basic conservation equations in space. The integral form of these equations, for conservation of mass, linear momentum, and total energy, are

$$\frac{\partial}{\partial t}\iiint_{volume}\rho dV=-\iint_{surface}\rho(\vec{u}\cdot d\vec{S}) \tag{2-1}$$

$$\frac{\partial}{\partial t}\iiint_{volume}\rho\vec{u}dV=-\iint_{surface}\rho\vec{u}(\vec{u}\cdot d\vec{S})+\iint_{surface}Td\vec{S} \tag{2-2}$$

$$\frac{\partial}{\partial t}\iiint_{volume}\rho edV=-\iint_{surface}\rho e(\vec{u}\cdot d\vec{S})+\iint_{surface}\vec{u}Td\vec{S} \tag{2-3}$$

where T is the stress tensor. For the hydrodynamic material models assumed for the numerical analyses of this investigation, T has the value $-p$ along the main diagonal, and zero everywhere else. Viscosity and thermal conductivity are neglected in these equations.

These equations are solved for each finite volume. A one point approximation is used to solve these equations (the value at the geometric center of the control volume), in conjunction with interpolated velocities and pressures at the faces of the finite volumes.

A first order "Donor-Acceptor" scheme is used for material transport. Transported quantities are subtracted from donor cells and added to the acceptor cells, based upon the donor cell values and the velocity at the common face. The face velocity for the face connecting finite volumes m and n is

$$\vec{u}_{face}=\frac{1}{2}(\vec{u}_m+\vec{u}_n) \tag{2-4}$$

and, during time step dt, the volume transport is

$$dV=\vec{u}_{face}\cdot d\vec{S}dt \tag{2-5}$$

The normal component of the face velocity determines which cell is a donor and which is an acceptor (i.e. in which direction flow occur). If, for example, cell m is the donor, the mass, momentum, and energy transport from element m to n is

$$dM=\rho_m dV=\rho_m \vec{u}_{face}\cdot d\vec{S}dt \tag{2-6}$$

$$d(M\vec{u})=\rho_m \vec{u}_m dV=\rho_m \vec{u}_m(\vec{u}_{face}\cdot d\vec{S})dt \tag{2-7}$$

$$de=\rho_m e_m dV=\rho_m e_m \vec{u}_{face}\cdot d\vec{S}dt \tag{2-8}$$

The solution in time is computed with this program using an explicit central finite difference method. With this method, a new time step size is calculated after each forward time step. This new time step is calculated such that the Courant criterion for a stable solution,

$$dt=S\frac{L}{u+c} \tag{2-9}$$

is satisfied, where S is a factor of safety, L is the smallest element dimension, c is the acoustic wave velocity within the element, and u is the partical velocity within the element. This is calculated for all elements, and the smallest value obtained is used as the new time step.

A complete time step algorithm consists of several phases. The momentum change

due to the impulse (from the face pressures) is calculated and used to update the velocity in each finite volume. Similarly, the work done by the pressure on each finite volume face is calculated and used to update the total energy for each finite volume. Mass, momentum and total energy transport across all faces are computed, and used to update these values in all finite volumes. The density and velocity in each finite volume are then updated (e.g. density equals new mass divided by fixed volume). The specific internal energy in each finite volume is computed based upon the new specific total energy and the new specific kinetic energy. And the pressure in each finite volume is updated using the new density and specific internal energy in the state equation.

To define a multimaterial Eulerian model with this computer program, several inputs are required. In addition to defining the geometry of the mesh, constitutive equation data must be input for the different materials to be used. Initial conditions must be assigned to all of the finite volumes in the model; for a multimaterial Eulerian problem these would include specification of what materials are initially in what finite volumes, and what the initial density and specific internal energy is in the different regions within the model. Any boundary conditions which are not to be left as the default "no flow" boundary condition must be specified. And, if the problem will use an explosive material, one or more detonation points, detonation velocities, and detonation times must be specified. Finally, the ending time for the analysis must be specified, and the program must be told precisely which output quantities are desired at what frequency.

III. BASIC EXPLOSION GAS BUBBLE BEHAVIOR

The effect of fluid compressibility and gas internal energy on the behavior of a free-field explosion gas bubble is investigated in this chapter. As discussed in the introduction, the basic characteristics of an explosion gas bubble are a rapid expansion to a much larger volume than the initial volume of the charge, a prolonged interval of time in this expanded state, and a rapid collapse back to a small volume. This oscillation cycle then repeats, but with a decreasing period between collapses and a decrease in the maximum volume to which the bubble expands.

In the first section in this chapter, the basic theoretical equations for the noncompressive motion of a free-field explosion gas bubble are developed. The second section describes the details of the numerical analysis models used in this investigation. Results from these analyses are presented in the last section.

A. THEORETICAL DEVELOPMENT

The classical expression for the motion of an explosion gas bubble in the absence of a nearby boundary surface neglects buoyancy resulting from pressure variation around the bubble and compressibility of the surrounding fluid. With these restrictions, the flow of fluid outside the bubble is radial, and conservation of energy gives

$$\frac{3}{2}\left(\frac{4\pi}{3}\rho_0 R^3\right)\left(\frac{dR}{dt}\right)^2+\frac{4\pi}{3}P_0R^3+E(R)=Y \tag{3-1}$$

where R is the radius of the bubble, ρ_0 is the density in the surrounding fluid, P_0 is the

hydrostatic pressure in the surrounding fluid, *E(R)* is the internal energy of the gas bubble when it has radius *R*, and *Y* is the total energy (a constant) (Cole, 1948, p.273).

In this expression, the first term represents the kinetic energy of the flow in the surrounding fluid, and the second term is the work done against hydrostatic pressure in expanding the bubble to radius *R*. By neglecting the internal energy of the gas, which has a relatively small value over much of the oscillation cycle of an explosion gas bubble, the total energy can be expressed as

$$Y=\frac{4\pi}{3}P_0R_{max}^3 \tag{3-2}$$

where R_{max} is the maximum radius of the bubble (Cole, 1948, p.274-275). This expression simply reflects the fact that the gas bubble must have a maximum radius when *dR/dt* is zero. Using equation (3-2) in equation (3-1), with *E(R)* taken as zero, equation (3-1) can be separated and integrated to give

$$t=(3\rho_0/2P_0)^{1/2}\int_{R_0}^{R}[(R_{max}/a)^3-1]^{-1/2}da \tag{3-3}$$

where R_0 is the initial radius of the gas bubble. By taking R_0 as zero (the initial radius of the bubble is much smaller than the maximum radius) and transforming and integrating equation (3-3), Willis (1941) arrived at the result

$$T=1.83R_{max}\left(\frac{\rho_0}{P_0}\right)^{1/2} \tag{3-4}$$

where T is the first oscillation period of the bubble. Substituting equation (3-2) into (3-4), and using the fact that the total energy Y is proportional to the weight W of the explosive charge gives

$$T=K_T\frac{W^{1/3}}{P_0^{5/6}} \tag{3-5}$$

where K_T is a constant particular to a given type of explosive. Equation (3-2) can be re-arranged to give

$$R_{max}=K_R\frac{W^{1/3}}{P_0^{1/3}} \tag{3-6}$$

where K_R is a constant particular to a given type of explosive. Equations (3-5) and (3-6) are the classical "semi-empirical" expressions for the scaling relationships for the first oscillation period and maximum radius of an explosion gas bubble.

B. NUMERICAL ANALYSIS MODELS

Two different numerical analyses were conducted for deep explosion gas bubbles in the absence of a nearby boundary surface. The first analysis was designed to correspond to one of a series of experiments conducted by Swift and Decius (1950) at the Woods Hole Oceanographic Institution during and shortly after the Second World War. These researchers conducted a large number of experiments to determine constants for the semi-empirical equations (3-5) and (3-6) above for different types of explosives. The tests were conducted at a deep depth in deep water, to minimize the effects of buoyancy and boundary surfaces.

The problem geometry for this analysis is shown in Figure 3-1. A very small (0.299

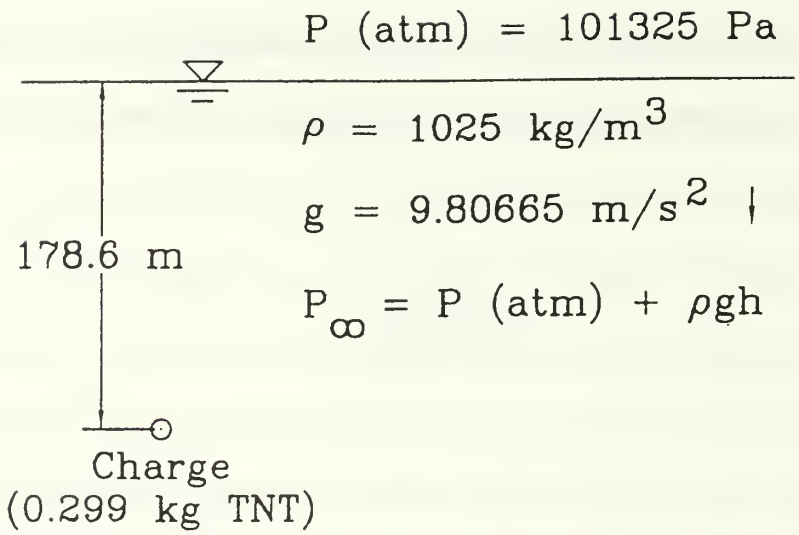

Figure 3-1. Geometry of Problem for Free-Field Bubble Analysis

kg TNT equivalent) charge was detonated at a depth of 178.6 m in seawater. The 0.299 kg TNT equivalent charge weight was calculated by Swift and Decius to account for the extra energy of the detonator and booster material used above the energy of the TNT in the main charge. This particular shot (shot G72F) was chosen from all of the shots conducted because the bubble oscillation period and maximum bubble radius from this experiment were closest to the mean values from all of the experiments. Although the experiments used cylindrical charges with a height to diameter ratio slightly larger than one, a spherical charge was modeled for this analysis.

In this experiment the maximum radius of the bubble was much less than the depth at which it was located. Thus, in the numerical analysis model for this problem, gravity was neglected and the pressure was assumed to be uniform in all directions from the charge. With this assumption, the problem is spherically symmetric. The seawater surrounding the charge

was treated as an invicid, irrotational fluid, and heat and mass transfer were assumed to be negligible over the time frame of the analysis. Herring (1950) has shown that the transfer of heat over one bubble oscillation cycle through conduction at the surface of the bubble constitutes a negligible fraction of the total energy of the explosion.

Since this problem as modeled has spherical symmetry, a one-dimensional model is appropriate. In order to model this one-dimensional problem with the three-dimensional analysis code MSC/DYTRAN, a tall, thin pyramid shaped region of fluid was used. This accounts for the increasing volume as one moves away from the charge. Boundary conditions on the sides of this fluid volume were made "no flow" conditions, as flow across the boundaries is precluded by the flow in adjacent fluid volumes. The analysis model used for this problem is shown in Figure 3-2.

At the apex of the pyramid shaped volume, a rectangular parallelpiped was used, with the equivalent volume a pyramid shaped volume would have. This avoids the use of a five sided pyramid shaped volume at the point, which is not a standard finite element shape. Rectangular parallelpiped shaped finite volumes were used to model the charge, and non-rectangular hexahedron finite volumes were used to model the remaining volume. Because the primary interest in this analysis was in the bubble behavior rather than the primary shock wave, only three finite volumes were used to model the charge.

In order to prevent reflection from the far end of the finite volume of fluid modeled from affecting the results during the duration of the analysis, a very large volume of surrounding fluid was modeled. A total of 999 finite volumes were used for this analysis model, with the radial length of individual elements increasing with increasing distance from

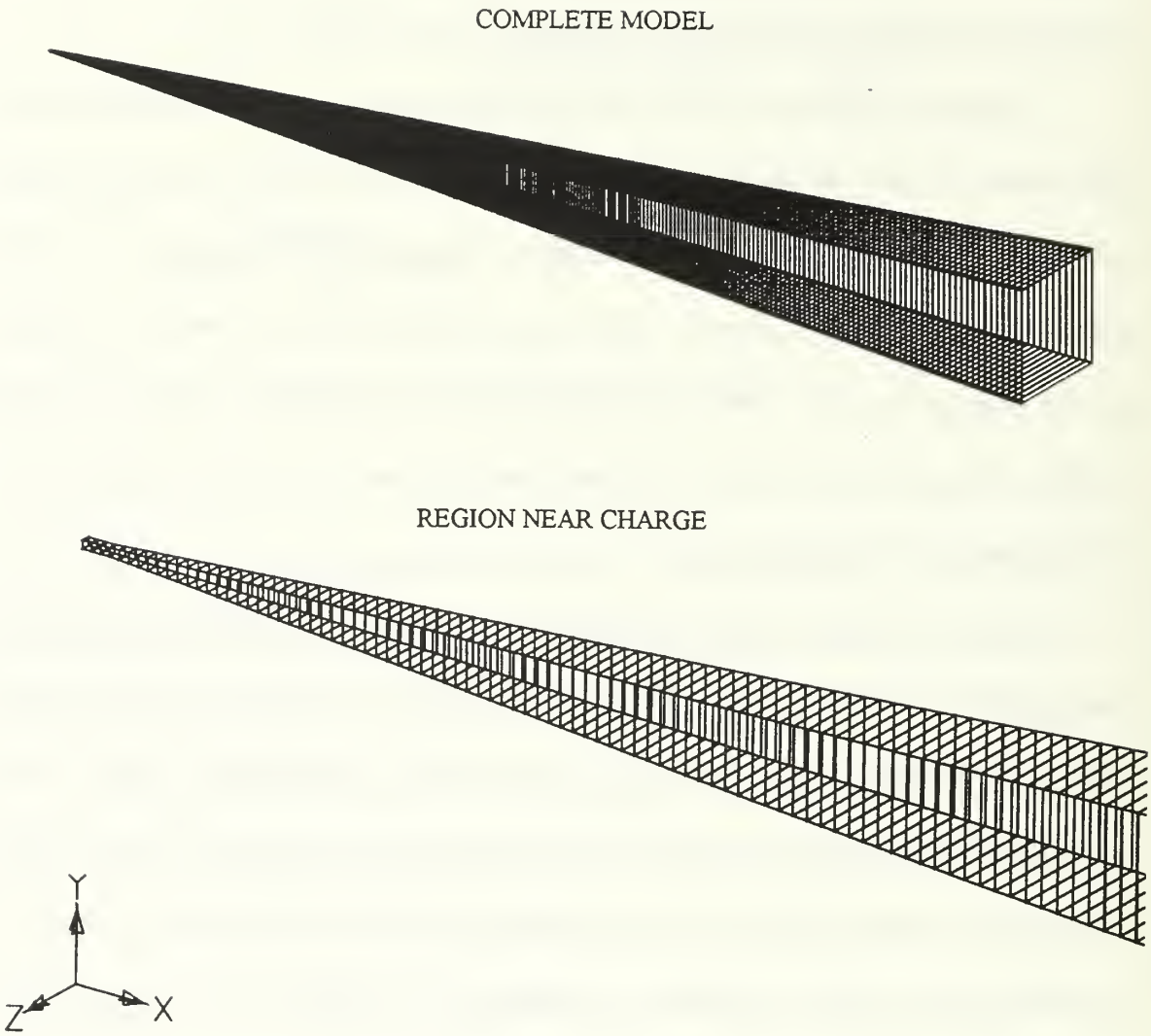

Figure 3-2. Numerical Analysis Model for 0.299 kg TNT Explosive Charge

the charge.

The TNT for this problem was modeled using a JWL state equation, with state equation parameters taken from the *Lawrence Livermore National Laboratory Explosives Handbook* (Dobratz, 1981). With this state equation, the pressure in the "burned fraction" of a charge is related to the specific internal energy and density by

$$p=A\left(1-\frac{\omega\eta}{R_1}\right)e^{-\frac{R_1}{\eta}}+B\left(1-\frac{\omega\eta}{R_2}\right)\exp^{-\frac{R_2}{\eta}}+\omega\eta\rho_0 E \qquad (3\text{-}7)$$

where $\eta=\rho/\rho_0$, ρ_0 is the initial density, E is the specific internal energy (per unit mass), and A, B, ω, R_1, and R_2 are constant parameters for the explosive. The "burned fraction" is just that portion of the explosive contained within a spherical detonation front traveling outward with detonation velocity d, which is another parameter characterizing the explosive. For TNT compressed to an initial density of ρ_0 of 1.630 g/cm^3, the JWL state equation parameters are (Dobratz, 1981):

$E = 4.29 \times 10^6$ J/kg
$A = 3.712 \times 10^{11}$ Pa
$B = 3.231 \times 10^9$ Pa
$\omega = 0.30$
$R_1 = 4.15$
$R_2 = 0.95$
$d = 6930$ m/s

In order to model the seawater in which this experiment was conducted, a polynomial state equation was used. This state equation relates the pressure in the fluid to its density ρ and specific internal energy E per unit mass by

$$p = a_1\mu + a_2\mu^2 + a_3\mu^3 + (b_0 + b_1\mu + b_2\mu^2)\rho_0 E \qquad (3\text{-}8)$$

where

$$\mu = \frac{\rho - \rho_0}{\rho_0} \qquad (3\text{-}9)$$

is the condensation and a_1, a_2, a_3, b_0, b_1, and b_2 are constants for the fluid. Constant for this state equation for seawater, for use at condensation values μ of up to 0.8, were determined by fitting available Hugonoit data from the literature to this state equation form, and adjusting the bulk modulus and density to the accepted values for seawater. The resultant state equation parameters were (Chisum and Shin, 1995)

$a_1 = 2.306 \times 10^9$ Pa
$a_2 = 8.432 \times 10^9$ Pa
$a_3 = 8.014 \times 10^9$ Pa
$b_0 = 0.4934$
$b_1 = 1.3937$
$b_2 = 0.0000$
$\rho_0 = 1025$ kg/m^3

The initial conditions given to the seawater in this problem were an initial condensation value of zero (initial density of 1025 kg/m^3), and an initial specific internal energy of 3750.4 J/kg. This initial specific internal energy was determined from equation (3-8); it represents the specific internal energy necessary to give the seawater an initial pressure equal to the hydrostatic plus atmospheric pressure for this problem. It was found necessary to use the initial specific internal energy rather than the condensation to set the initial pressure, because seawater is so incompressible that there is only a minuscule density change at this depth, and significant round off errors would be introduced by setting the initial

pressure with the condensation.

The second model geometry analyzed was similar to Figure 3-1, except that an initial charge depth of 1000 m and an initial TNT charge of 3.5 kg was used. This corresponds to an initial charge radius of 8.0 cm. The objective of this analysis was to examine the flow characteristics in the surrounding fluid over one oscillation of the bubble. For this reason, uniform element spacing in the radial direction was used. A pyramid shaped volume of fluid was again used. In this case, the fluid was only modeled out to a distance of 16 m, and a simplified "non-reflecting" boundary condition was placed on the last element. This boundary condition was that the flow across the face of the element at the boundary would have the same values as in that element.

The radial element spacing used was 0.125 cm, and a total of 12800 finite volumes were used. It was not necessary to use this many elements to get a "grid independent" solution, but the use of a fine mesh better illustrates the characteristics of the shock wave. The computer program used utilizes artificial bulk viscosity to control oscillations behind shock waves, and this smears the shock front over a number of elements. Mass, energy, and momentum are still conserved, but the shock wave doesn't look as steep. Thus, using more elements makes the shock wave "look" more like a shock wave, since it is smeared over a smaller distance.

C. NUMERICAL ANALYSIS RESULTS

As stated in the last section, the first of the problems analyzed corresponded to an experiment conducted by Swift and Decius. Figure 3-3 shows the predicted radius time history from this analysis, and the first maximum bubble radius and period measured from the

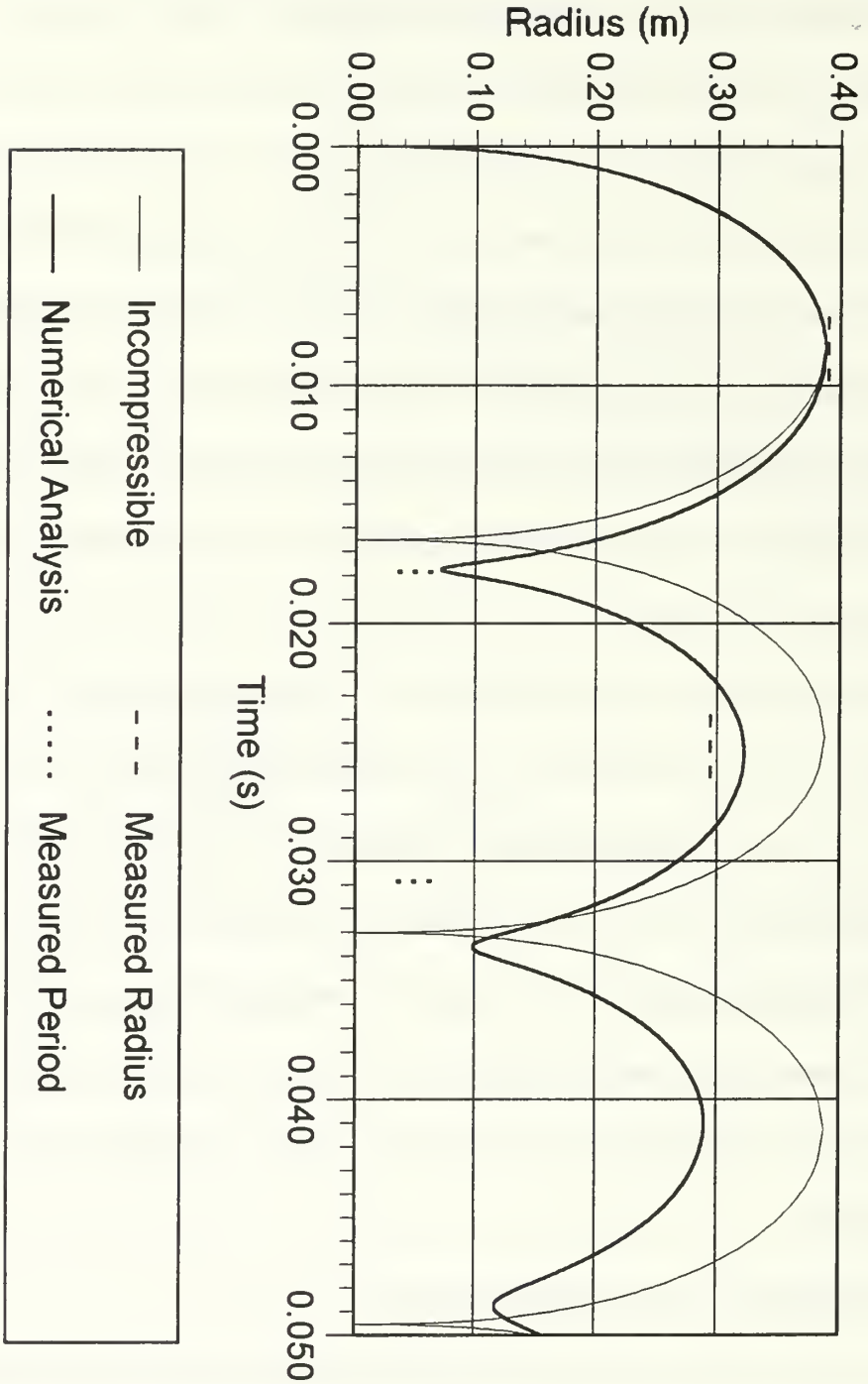

Figure 3-3. Radius Time History for 0.299 kg TNT Charge Detonated at 178.6 m

experiment. This plot shows excellent agreement between the analysis results and the experimental measurement. Also shown on this plot, for comparison purposes, is the radius time history curve generated from step-by-step numerical integration of equation (3-3), which neglects both the internal energy of the gas bubble and fluid compressibility. This curve is seen to agree quite well with the numerical analysis curve up until the bubble reaches maximum volume, but to begin diverging from there.

It is seen in Figure 3-3 that the numerical analysis predicts the bubble radius and oscillation period to decrease in subsequent oscillations. This is due to the radiation of a bubble pulse when the bubble collapses. This effect cannot be generated without including fluid compressibility.

Figure 3-4 shows the pressure, impulse, and fluid particle velocity time histories, at a point located two maximum bubble radii from the center of the charge. This figure illustrates that, although the peak pressure in the first bubble pulse is much less than the peak shock wave pressure, the impulse generated by the bubble pulse is still large because of its longer duration.

In their experiment, Swift and Decius also measured the second period and second maximum radius for this shot. Their measurements indicated that the second maximum radius was 11.6 inches (about 29.5 cm), and that the measured time for the second bubble minimum was 30.85 msec. These results indicate that an additional energy loss, above that due to acoustic radiation, occurred in this experiment, since acoustic radiation was accounted for in the numerical analysis for this problem.

One possible explanation for this in that the bubble surface was unstable near the

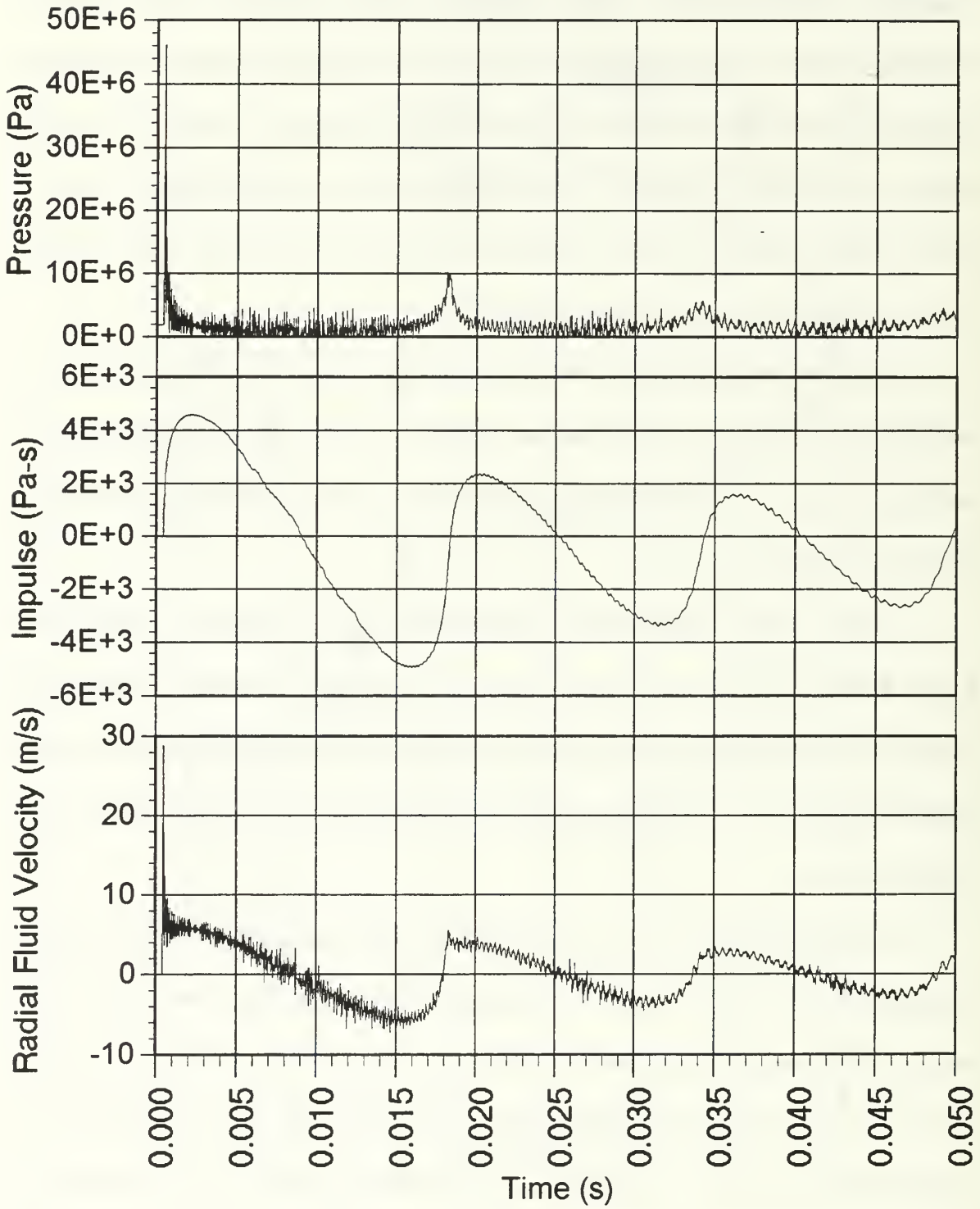

Figure 3-4. Numerically Predicted Pressure, Impulse, and Velocity Time History for 0.299 kg TNT Charge Detonated at 178.6 m, at a Point Two Maximum Bubble Radii From the Charge Center

minimum volume. Hicks (1970a) has noted that photographs of non-migrating bubbles typically show numerous needle-like water jets protruding into the bubble surface when the bubble is near minimum radius, and that this "spray" of water could significantly cool the hot bubble gases.

In the second free-field numerical analysis, the flow external to the bubble was examined. Figure 3-5 shows the bubble radius time history for this analysis, and Figure 3-6 shows the variation of the internal energy of the bubble as a function of time. The internal energy is seen to rapidly decrease from its initial value as the bubble expands, and then to increase moderately as the bubble is compressed by the surrounding fluid.

Figures 3-7, 3-8, and 3-9 show the pressure in the fluid at 1 msec intervals. Because the shock wave is radiating spherically, the peak pressure of the shock wave decreases rapidly with increasing distance. The pressure behind the shock front drops below hydrostatic pressure, and this low pressure region extends for a considerable distance from the bubble by 5 msec, when the bubble is near maximum radius. Also, by 5 msec there is a second sharp drop in the pressure behind the shock wave, and after 5 msec this sharp drop extends further and further into the fluid.

This is caused by the reversal of flow in a portion of the fluid. The fluid immediately behind the shock front is still moving outward, but the fluid near the bubble surface is moving inward as the bubble contracts. As time goes on, fluid further and further away from the bubble begins moving inward. By the time the bubble reaches minimum volume, the pressure near the bubble is significantly higher than even the primary shock wave. As the bubble reaches minimum volume and begins expanding again, a moderately low pressure but long

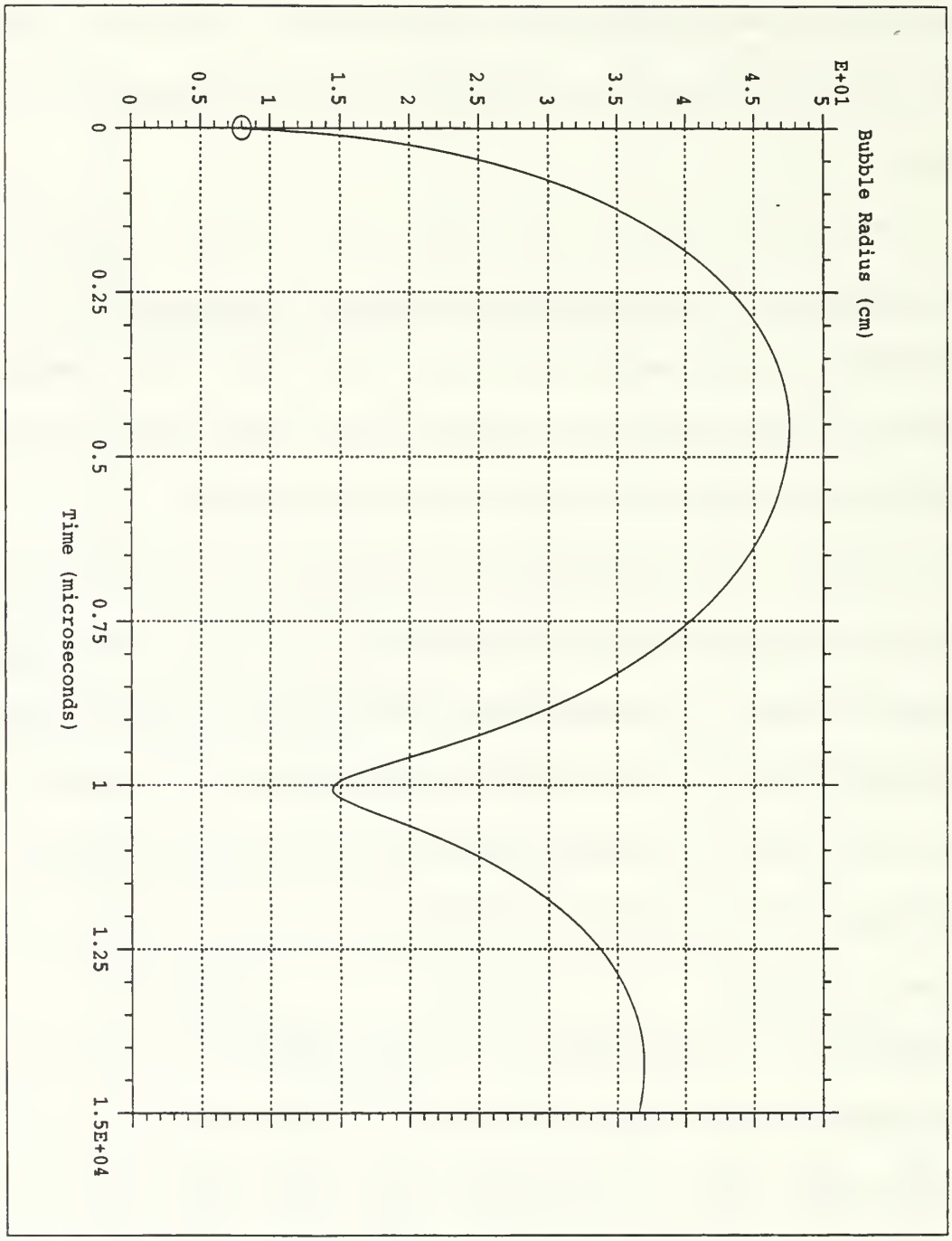

Figure 3-5. Predicted Bubble Radius Time History for 3.5 kg TNT Charge Detonated at 1000 m

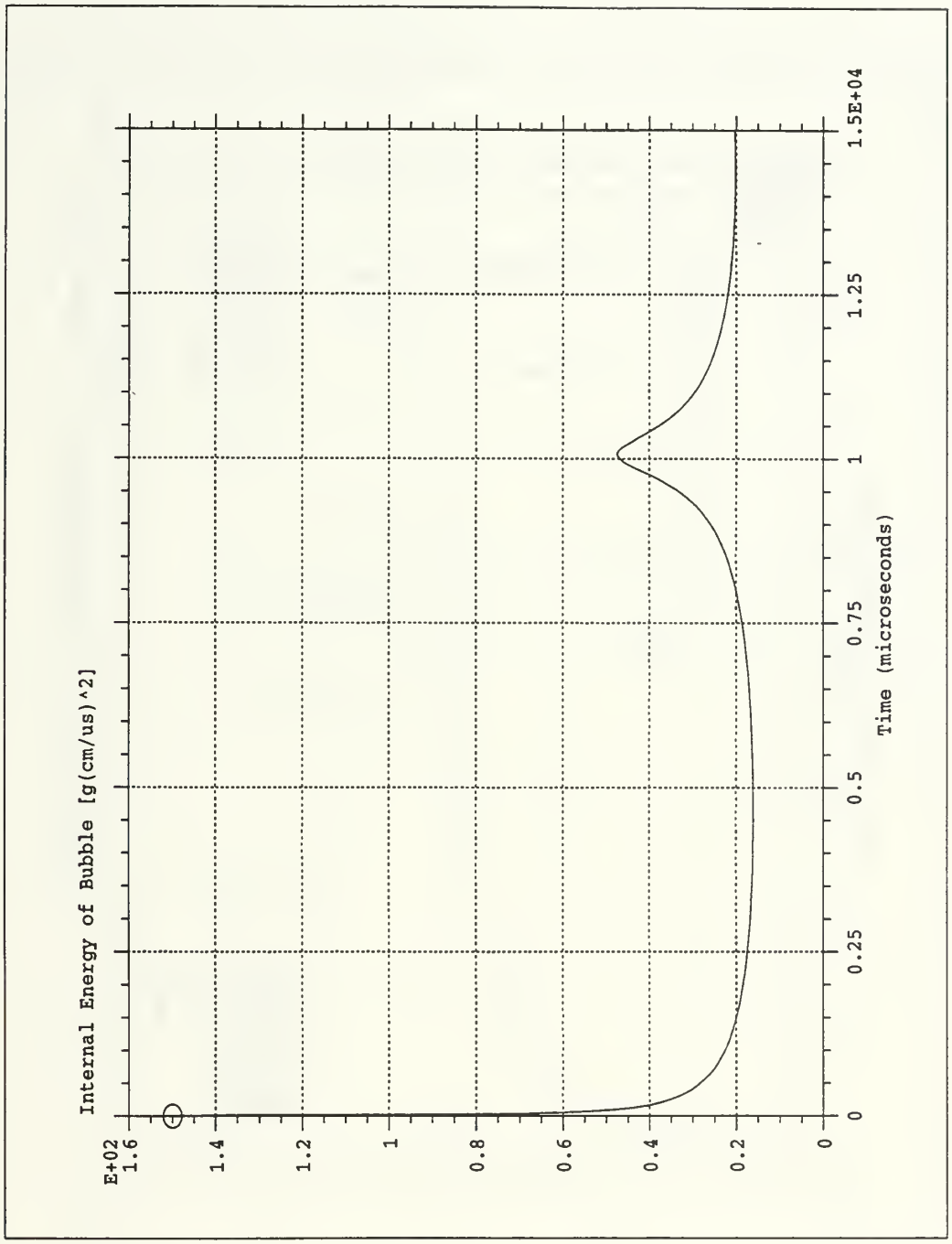

Figure 3-6. Predicted Bubble Internal Energy Time History for 3.5 kg TNT Charge Detonated at 1000 m

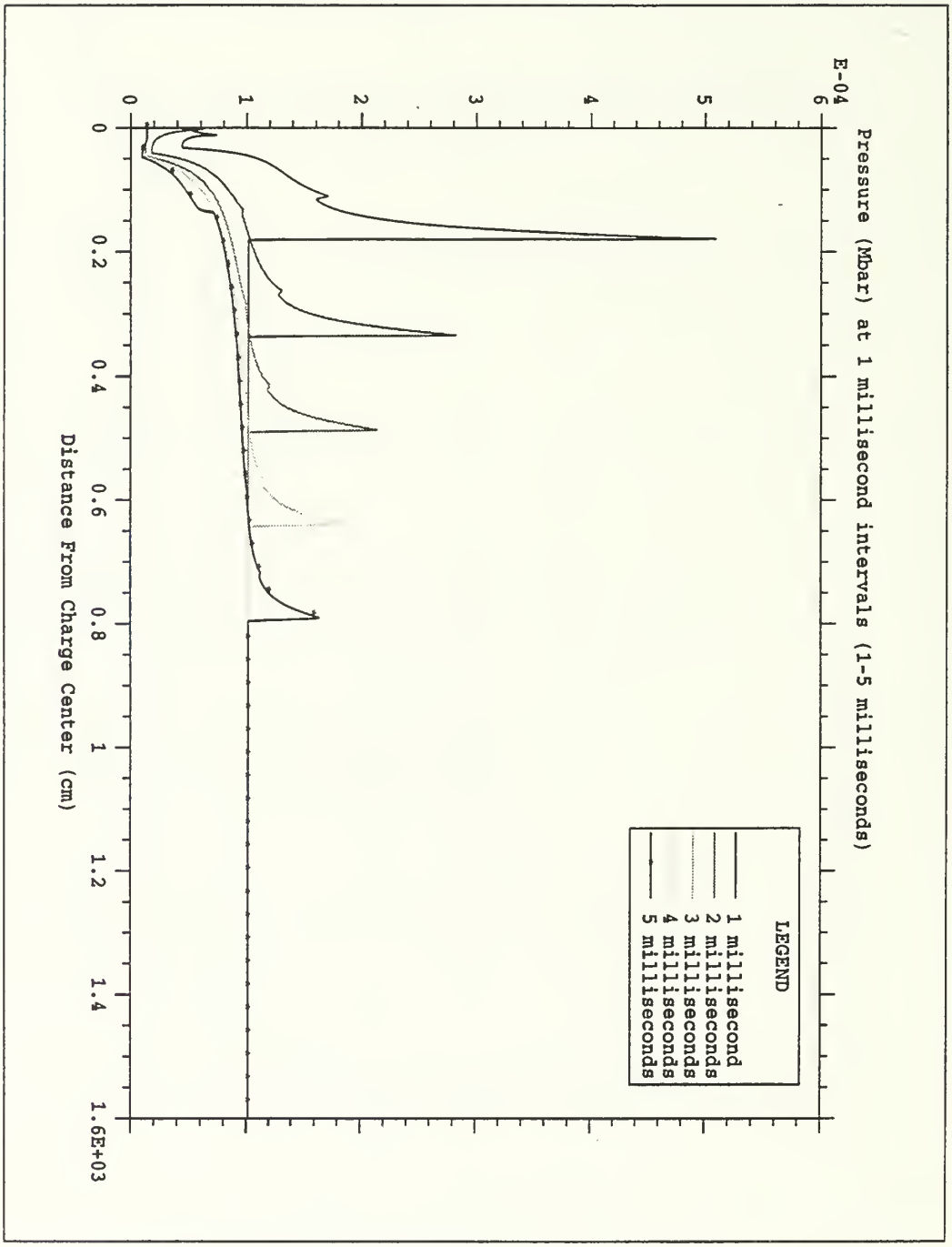

Figure 3-7. Pressure Distribution From 1 msec Through 5 msec After Detonation of a 3.5 kg TNT Charge at a Depth of 1000 m

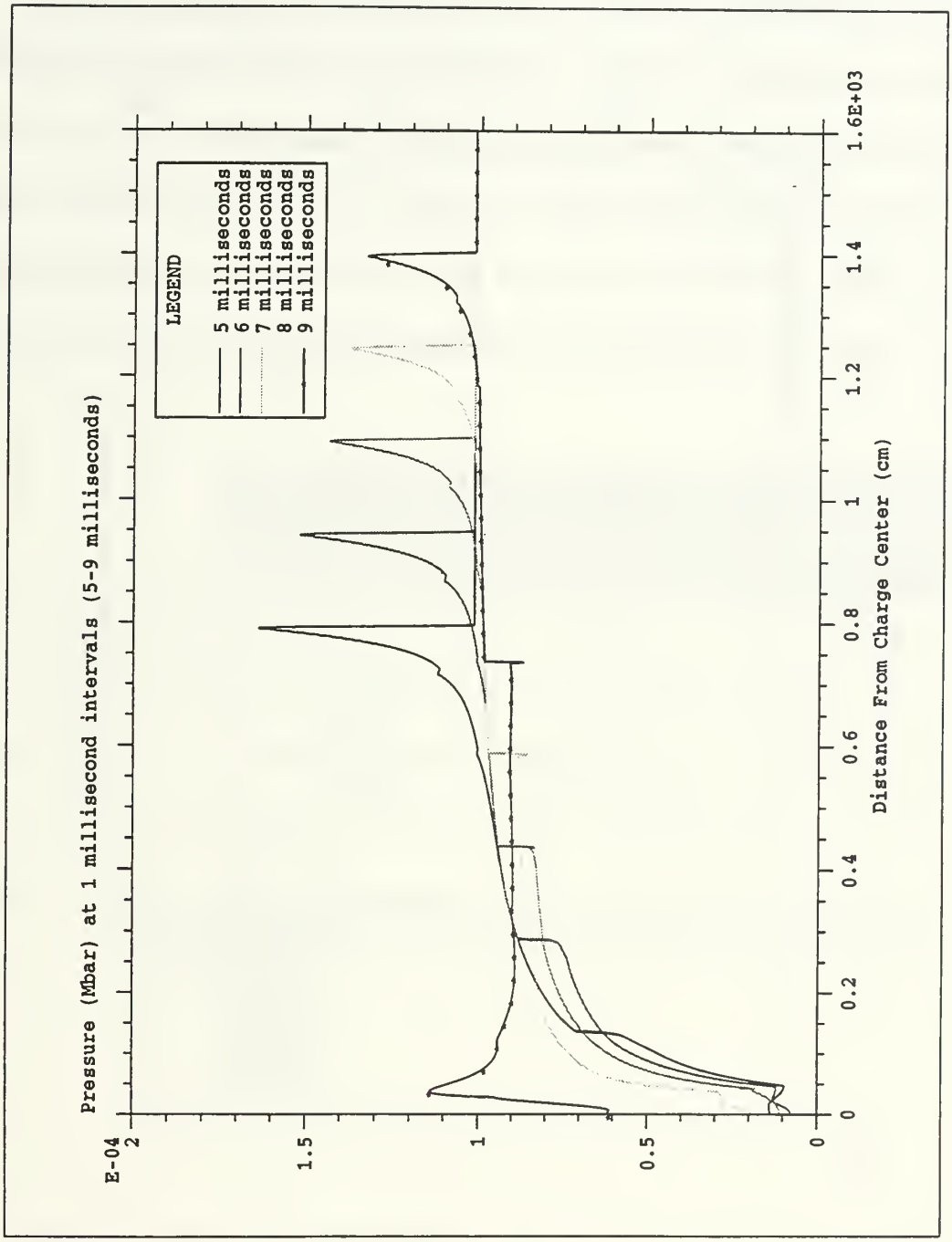

Figure 3-8. Pressure Distribution From 5 msec Through 9 msec After Detonation of a 3.5 kg TNT Charge at a Depth of 1000 m

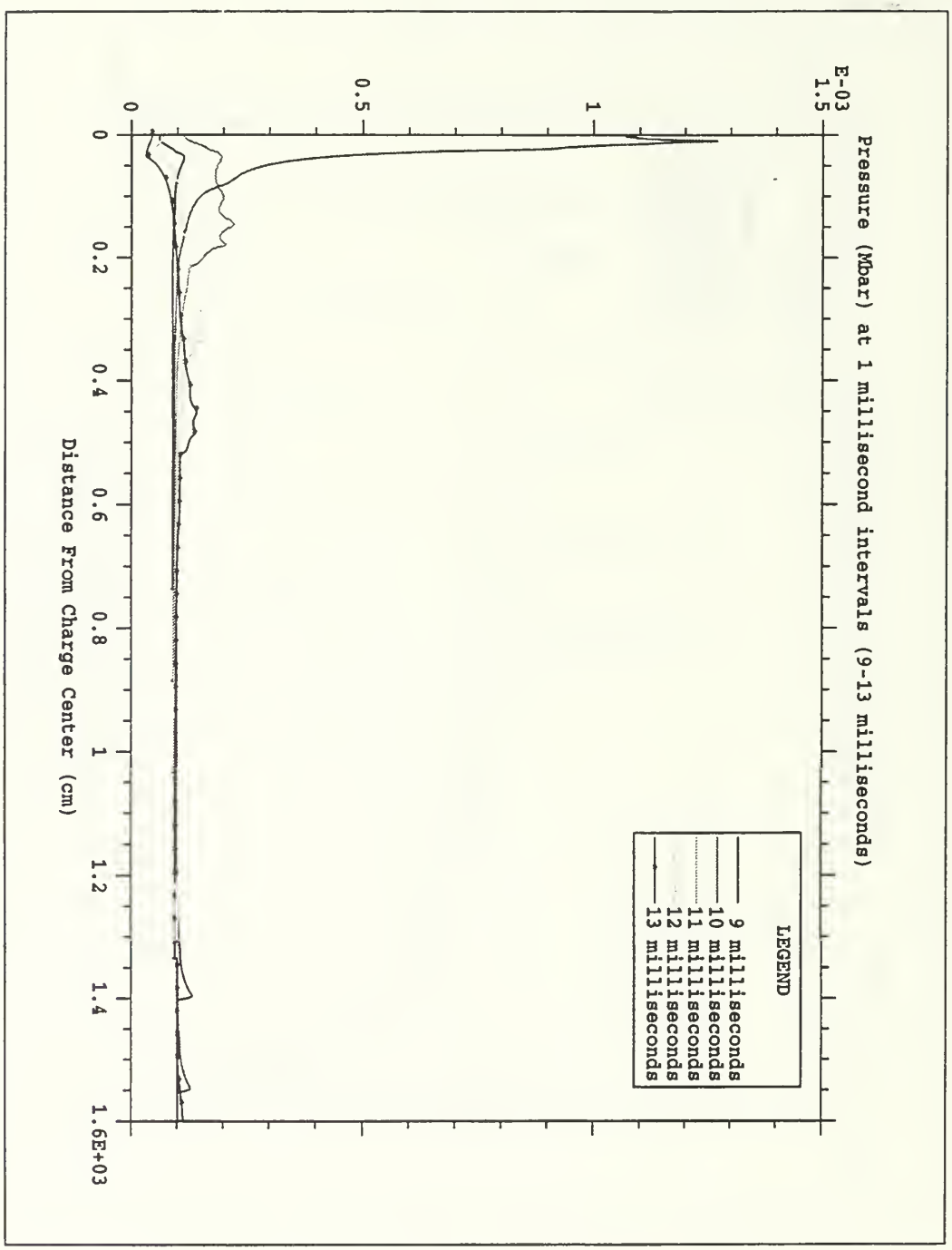

Figure 3-9. Pressure Distribution From 9 msec Through 13 msec After Detonation of a 3.5 kg TNT Charge at a Depth of 1000 m

duration bubble pulse begins traveling outward away from the bubble.

Table 3-1 compares the results between the experiment conducted by Swift and Decius and the current numerical analysis predictions. Extremely good agreement is seen for the first maximum bubble radius and period, while the second maximum bubble radius and period are appreciably less. The solution computed using the noncompressive theory neglecting the internal energy of the gas bubble was 8% lower than the actual period. Internal gas energy and fluid compressibility thus have an observable effect on the results.

	EXPERIMENTAL MEASURMENT	NUMERICAL ANALYSIS	% ERROR
R(1)	39.1 cm	38.8 cm	0.8
T(1)	17.85 msec	17.77 msec	0.4
R(2)	29.5 cm	32.2 cm	9
T(2)	13.00 msec	15.85 msec	22

Table 3-1. Comparison Between Experimental and Numerical Analysis Results For First and Second Maximum Bubble Radius and First and Second Bubble Period.

IV. EXPLOSION GAS BUBBLE BEHAVIOR NEAR SIMPLE BOUNDARIES

A. INTRODUCTION

While free-field explosion gas bubbles dynamic behavior has been discussed in the previous chapter, practical problems typically involve the interaction of these bubbles with boundary surfaces. As discussed in the introduction, additional phenomena are observed when an explosion gas bubble is generated near a boundary surface. These include a change in the oscillation period of the bubble, and migration of the bubble from its initial position in the fluid medium.

These phenomena will affect the damage caused by whipping of the hull girder of a naval vessel. The time interval between arrival of the primary shock wave and the first bubble pulse can be very near or equal to the fundamental period of the whipping mode of vibration of the hull girder, significantly increasing the whipping mode response of the vessel. Since the bubble pulse is generated at the conclusion of the contraction phase of the bubble oscillation, the period of this oscillation is obviously important. The migration of the bubble towards or away from a boundary during this oscillation is also important, as this determines the origination point of the bubble pulse. This affects both the arrival time of the bubble pulse and its magnitude, as the magnitude decreases with increasing distance.

Since the available analytical models are known to not give quantitatively accurate results for the effects of boundary surfaces on underwater explosion gas bubbles, a number of numerical analyses using Eulerian finite volume meshes were conducted. These included a free-field analysis in which no nearby boundary was present, a series of analyses in which

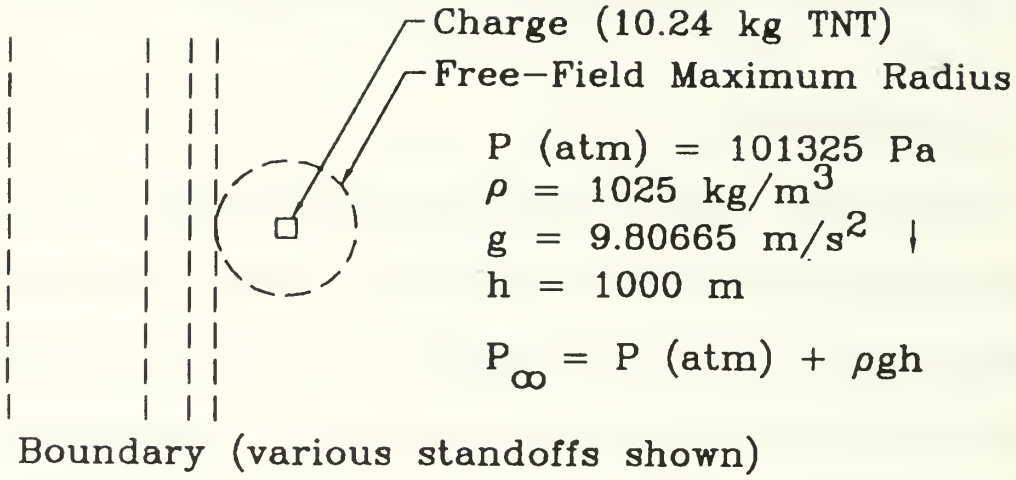

Figure 4-1. Geometry of Problem for Bubble Near Boundary Analyses

a plane infinite rigid boundary was located at various standoff distances from the charge, and a series of analyses in which a plane infinite free (constant pressure) surface was located at various standoff distances from the charge.

B. NUMERICAL ANALYSIS MODELS

The basic problem geometry for these analyses consists of a 10.24 kg cylinder of TNT, with a height to diameter ratio of one, located near an infinite plane boundary at a depth of 1000 m, as shown in Figure 4-1. Underwater explosion experiments also typically use cylindrical charges, for practical reasons. As in the free-field analyses described in the previous chapter, the choice of a deep charge depth serves to significantly reduce the period of oscillation of the bubble, and hence the analysis time.

A deep charge depth also serves to simplify the analyses, as at a deep depth the variation in hydrostatic pressure in the surrounding fluid for a given depth change is

proportionately much smaller than at a shallow depth. The hydrostatic pressure in the fluid near a deep charge can thus be approximated as having a uniform value, the hydrostatic pressure at the depth of the charge, provided that the overall dimensions of the explosion gas bubble is much smaller than the depth of the charge. This was the assumption made for the analyses described in this chapter, for which the maximum bubble radius was less than 0.1% of the depth of the charge.

The migration due to gravity can be separated from the migration caused by the presence of plane boundary surfaces, for cases in which the boundary surfaces have no component normal to the direction of the gravitational acceleration. Furthermore, deep explosion gas bubbles are known to experience little vertical migration due to gravity (Hicks, 1970a). Thus, gravity can be neglected except for its effect on the hydrostatic pressure in the surrounding fluid. This permits separation of the effects of gravity from the effects of a boundary surface, facilitating investigation of the influence of the boundary surface on the dynamic behavior of the bubble. For the same purpose, Blake and Gibson (1981) have conducted experiments using spark generated vapor bubbles with the entire experimental apparatus in free fall.

For these analyses, the cylindrical charge is assumed to have its axis normal to the plane boundary surfaces. With this orientation, the problems analyzed are axially symmetric, with the symmetry axis being the axis of the charge. To analyze these axially symmetric geometries using the three-dimensional code MSC/DYTRAN, wedge shaped volumes comprising two degrees of arc were used.

Figure 4-2 illustrates the overall shape of the volume of fluid modeled, for the free-

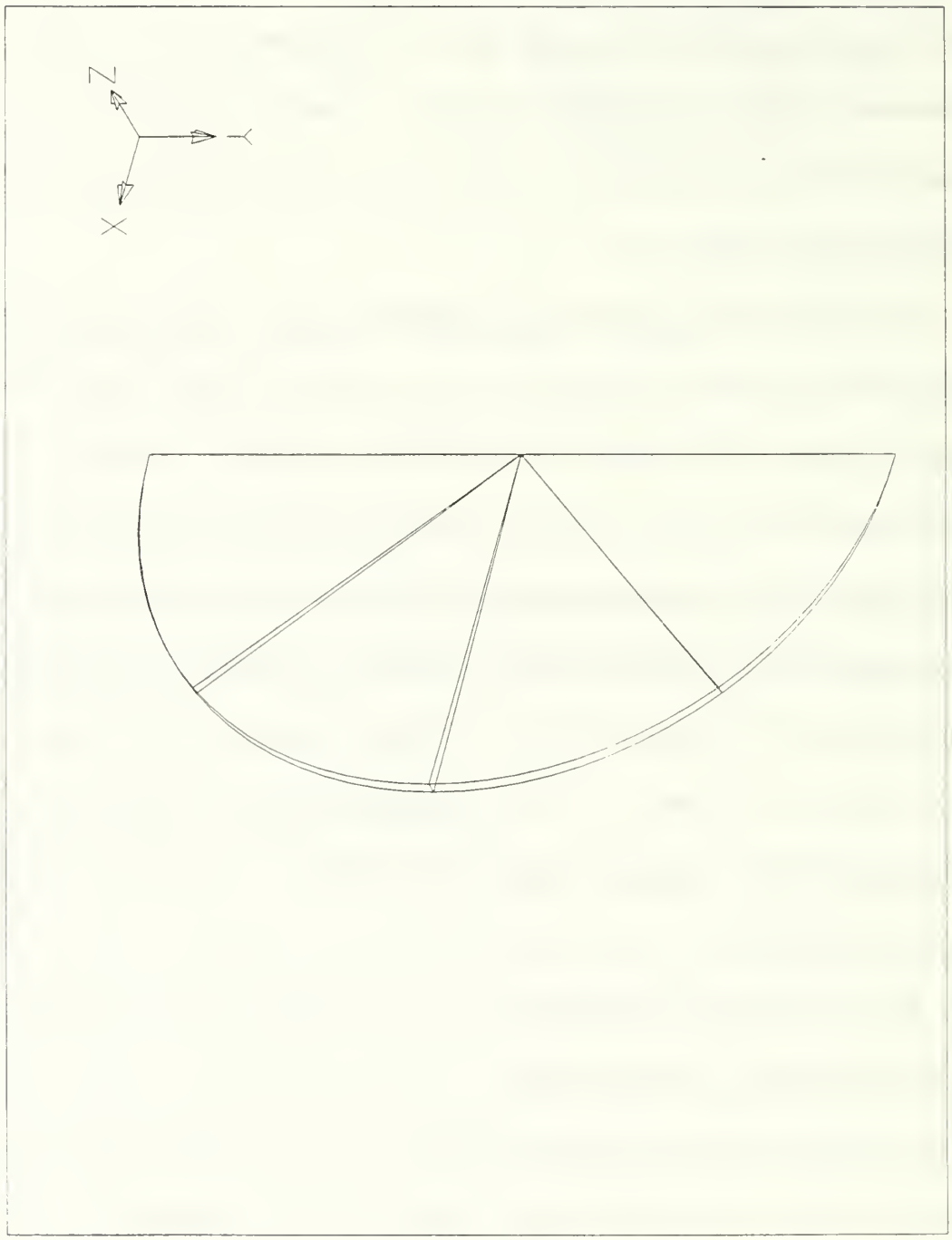

Figure 4-2. Overall Geometry of Analysis Model for Free-Field Analysis

field analysis in which no boundary surface is present. The vertical line oriented in the *y* direction in this model is the axisymmetric symmetry axis of the problem. The boundary conditions imposed on the two semi-circular areas, lying in the planes oriented at +/- 1 degree about the axisymmetric symmetry axis from the *x-y* plane, are "no-flow" (rigid wall) boundary conditions, as flow across these boundaries is precluded by the flow in adjacent wedge segments (not modeled or shown).

As discussed in the section in the previous chapter describing free-field analysis results, the dynamic behavior of underwater explosion gas bubbles is influenced by the conditions in the surrounding fluid adjacent to and at some distance from the bubble. Thus, a large volume of surrounding fluid was modeled in these analyses. This acts both to incorporate the necessary fluid and to avoid having to specify particular boundary conditions at the remote boundary of the finite volume of modeled fluid. This remote boundary was simply made a "no-flow" (rigid wall) boundary, with the distance to the boundary being made so great that shock wave reflection from it could not affect the analyses during the time frame of the analyses. For the free-field model volume shown in Figure 4-2, this remote boundary is the curved area connecting the semi-circles rotated +/- 1 degree about the *y*-axis from the *x-y* plane. These semi-circles are located at a distance of 400 m from the detonation point; as discussed below, an increased element size is used far away from the center of the charge, so that relatively few extra elements are needed to model fluid very remote from the center of the charge.

The finite volume meshes used for the analyses described in this chapter were developed to meet several goals. It was important that the results obtained be independent

of the mesh used to obtain them, i.e. that the solution was "grid independent." This goal could be met simply by using a large number of equal sized elements (finite volumes) for the analyses. However, if carried to extremes this practice is in direct conflict with other goals that a practical model must meet; that is, that the model must be able to run using a reasonable amount of computer resources (such as memory and storage space for results), and that the model must run to completion in a reasonable amount of time. It was also considered important that the results be independent of the shape of the elements used in the area near the charge, even if the bubble migrated during the analyses. A considerable amount of effort was expended in order to meet all of these goals for the analyses described in this chapter.

During the development of meshes for these analysis, it was eventually determined that a mesh consisting of three separate regions could meet these goals. From a two-dimensional perspective, the central region of these meshes consists of a rectangular region with square elements. This configuration allows elimination of element shape as a factor, since if this element geometry can still produce spherically shaped bubbles and the bubbles remain within this region during the analyses, then the shape of the element was not important in determining the results. The second region is a transition from this square element region to a spherically diverging type of region, which is necessary if the total number of elements is to be kept to a reasonable value. The third region is the spherically diverging type region, in which the dimensions of the element increase with increasing distance from the center of the charge, which, again, serves to limit the number of elements to a reasonable value.

The use of this spherically diverging region is supported and suggested by the results

from the previous chapter, where it is seen that characteristics of the flow in the surrounding fluid are changing much slower in the remote fluid than in the fluid near the charge. As the purpose of the analyses described in this chapter is to determine the dynamic behavior of the bubble rather than the primary shock wave, it does no harm if the primary shock wave is spread over a larger region. And since a reasonable number of elements is still used in the circumferential direction (in the free-field model, 34 elements over 45 degrees, i.e. about 1.3 degrees per element), this element geometry should still be valid for the analyses in which a boundary surface is present, and there is some circumferential change in the flow field.

The dimensions of the rectangular (square meshed) region used was several times the maximum bubble radius of the charge. This was found to be necessary to eliminate mesh reflection affects on the bubble radius-time history for the free-field analysis. This meshing in sufficient to capture the important effects which occur within a short distance of the charge, as seen in the previous chapter.

The mesh transition region provides a transition from the square meshed central region to the spherically diverging outer region, and reduces the number of elements in the circumferential direction per unit circumferential distance. This reduction is important in limiting the total number of elements needed for the analyses. Figure 4-3 shows the geometry of the central region and transition region for the free-field analysis model; this is just an expanded view of Figure 4-2, in the region in which the charge is located.

To insure a grid independent solution, free-field analyses were conducted for which the square element dimensions in the central region were 2.5 cm and 3.333 cm (with slight differences in the gross dimensions of the central region (247.5 cm and 250 cm width)), and

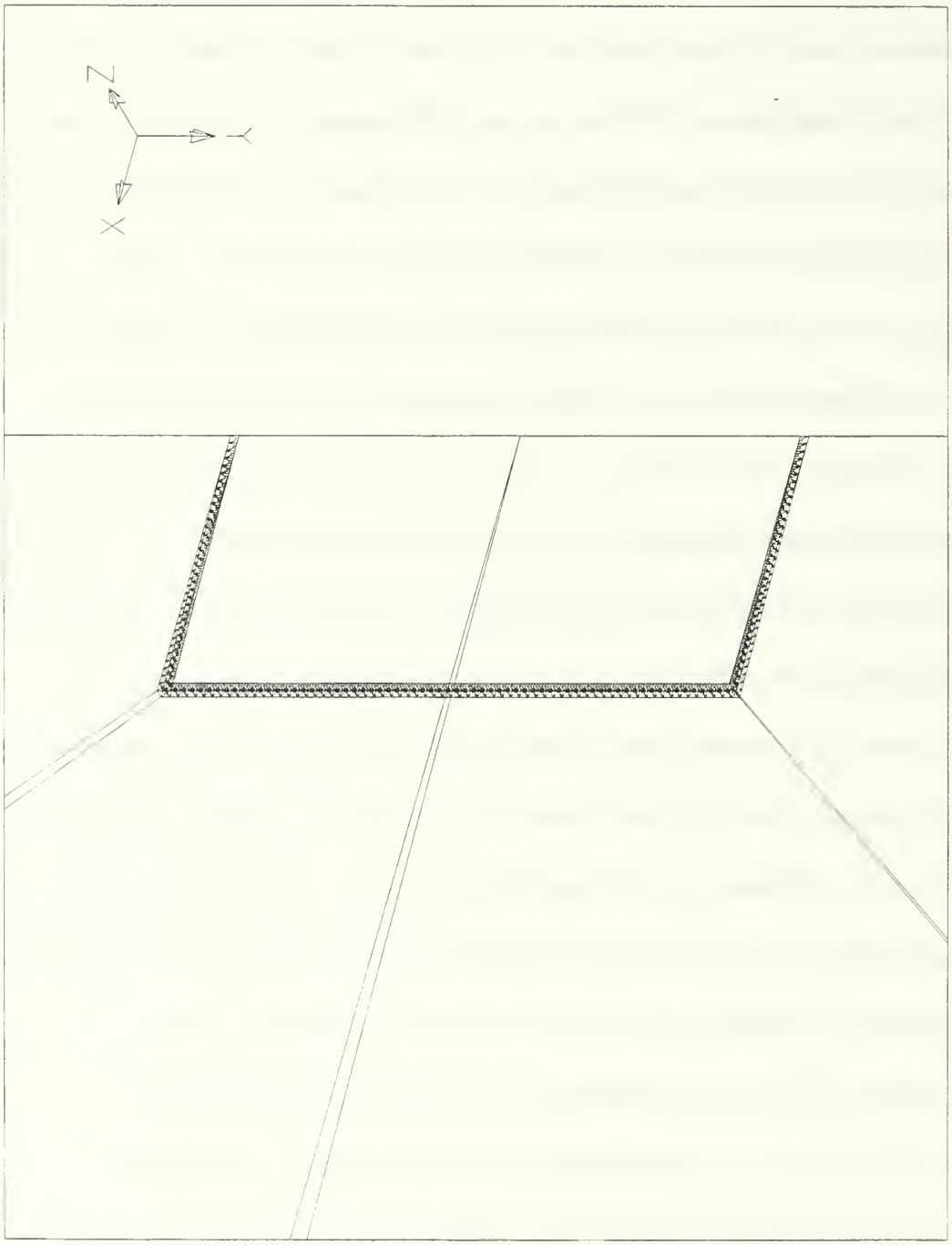

Figure 4-3. Geometry of Analysis Model for Free-Field Analysis in Area Near Charge

the bubble radius versus time curves were found to lie on top of each other. It was concluded from these results that the 2.5 cm square dimension solution was a grid independent solution for the free-field case. It was then assumed that this meshing would be adequate for analyses involving a nearby boundary surface, since the meshing for these analyses was kept similar to the free-field meshing.

Figure 4-4 shows the gross finite volume analysis mesh from a two-dimensional perspective, for the free-field analysis. Figure 4-5 shows the central rectangular region of this mesh, and the transition from this central region to the outer (spherically diverging) region. The total number of finite volumes (elements) used for this analysis is 47340. The central (square meshed) region uses 19602 elements, the transition region uses 338 elements, and the outer region uses the remaining 27200 elements. In this outer region, the mesh is designed such that the dimensions of individual elements remain nearly equal as the mesh diverges from the central region.

The maximum bubble radius predicted by the free-field analysis was about 70.65 cm, and the first bubble period from this analysis was about 14.47 msec. These values were used to assist in quantification of the results for analyses which included a boundary surface. For analyses involving a boundary surface, lengths are given in terms of the non-dimensional standoff distance h^*, where h^* is the standoff distance from the center of the charge to the nearest point on the boundary in units of maximum free-field gas bubble radii. Times are given in terms of the non-dimensional period T^*, where T^* is the time in units of bubble free-field first oscillation periods.

The free-field axisymmetric model was used as the starting point for other analysis

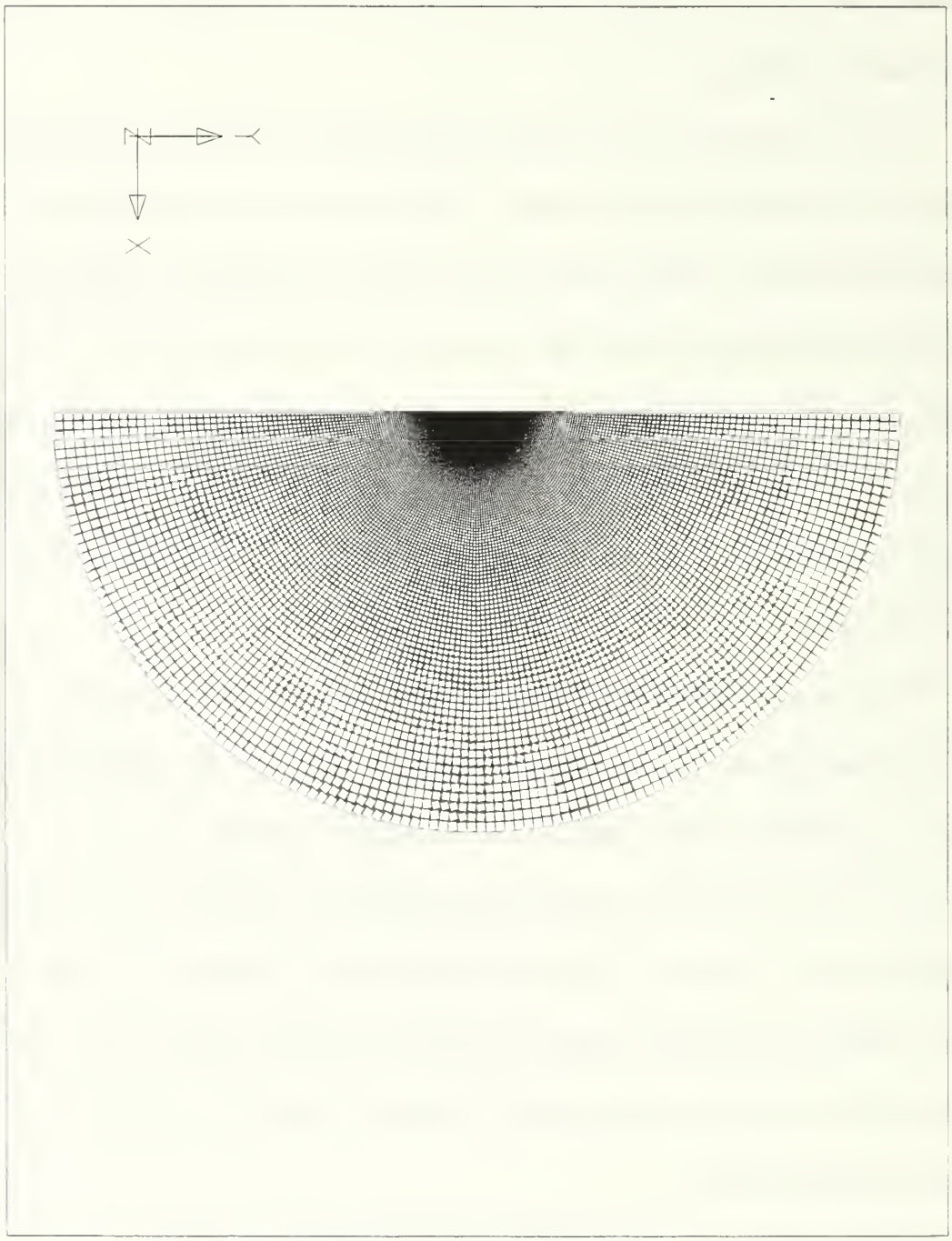

Figure 4-4. Overall Finite Volume Analysis Mesh for Free-Field Analysis

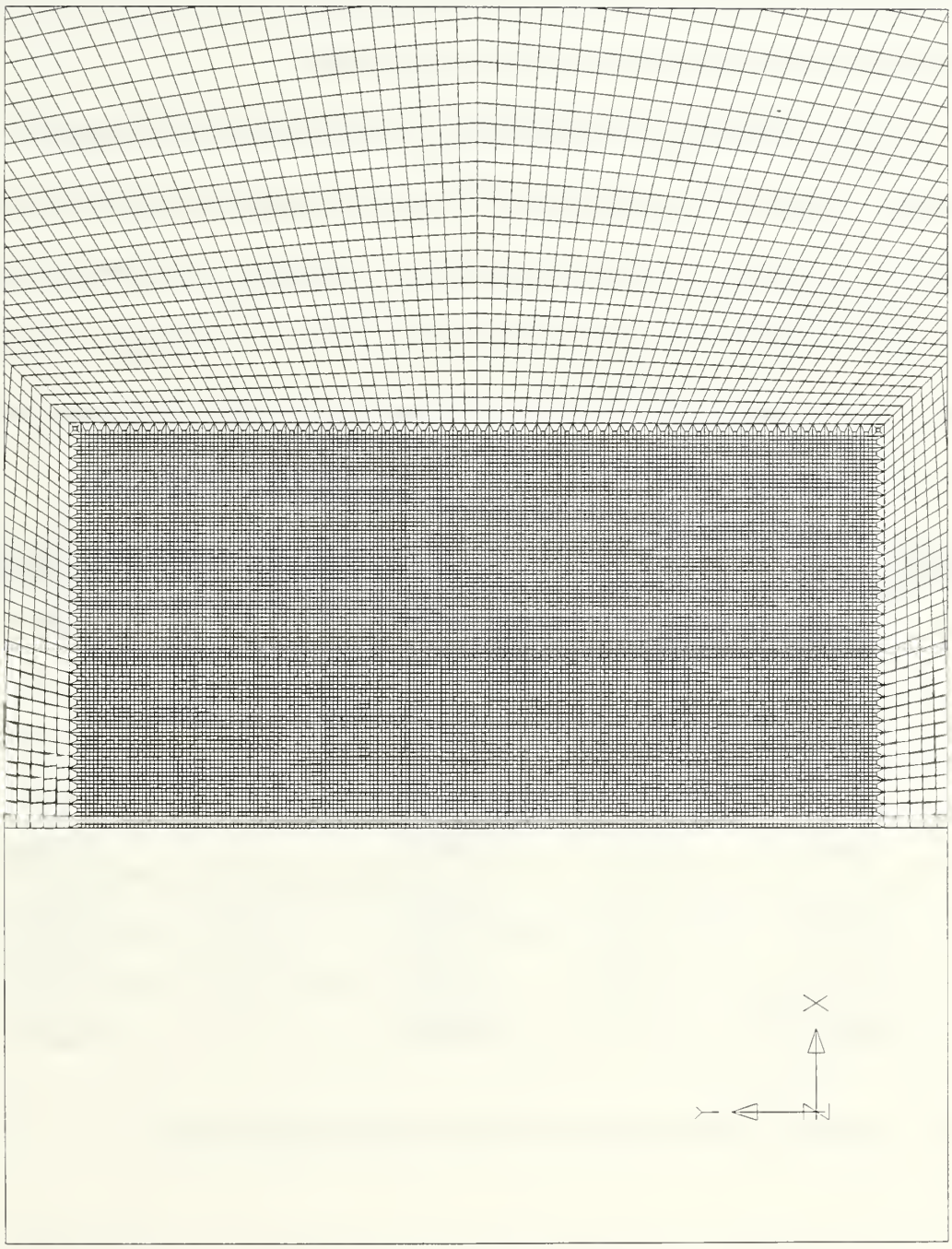

Figure 4-5. Finite Volume Analysis Mesh for Free-Field Analysis in Area Near Charge

models involving a rigid wall boundary and a constant pressure surface. Analyses were conducted at standoff distances of h^* ranging from 1.062 to 4.034, for both types of boundaries. These h^* values correspond to standoff distances from the center of the charge to the boundary ranging from 75 cm to 285 cm, respectively.

Table 4-1 summarizes the characteristics of the models used in these analyses. The total number of finite volumes (cells) used in these models ranged from 28680 (for the h^* equal to 1.062 analyses) to 42708 (for the h^* equal to 4.034 analyses). The models for these analyses were similar to the free-field model described above, but with additional elements present below what was an additional symmetry plane for the free-field model (bisecting the axis of the charge).

Standoff Distance (cm)	h*	Number of Finite Volumes
75.0	1.062	28680
82.5	1.168	29181
97.5	1.380	30183
120.0	1.698	31686
142.5	2.017	33189
187.5	2.654	36195
285.0	4.034	42708
(Free-Field)	(Infinity)	47340

Table 4-1. Summary of Characteristics of Finite Volume Analysis Models

Figure 4-6 shows the geometry of a typical model used in these analyses from a three-

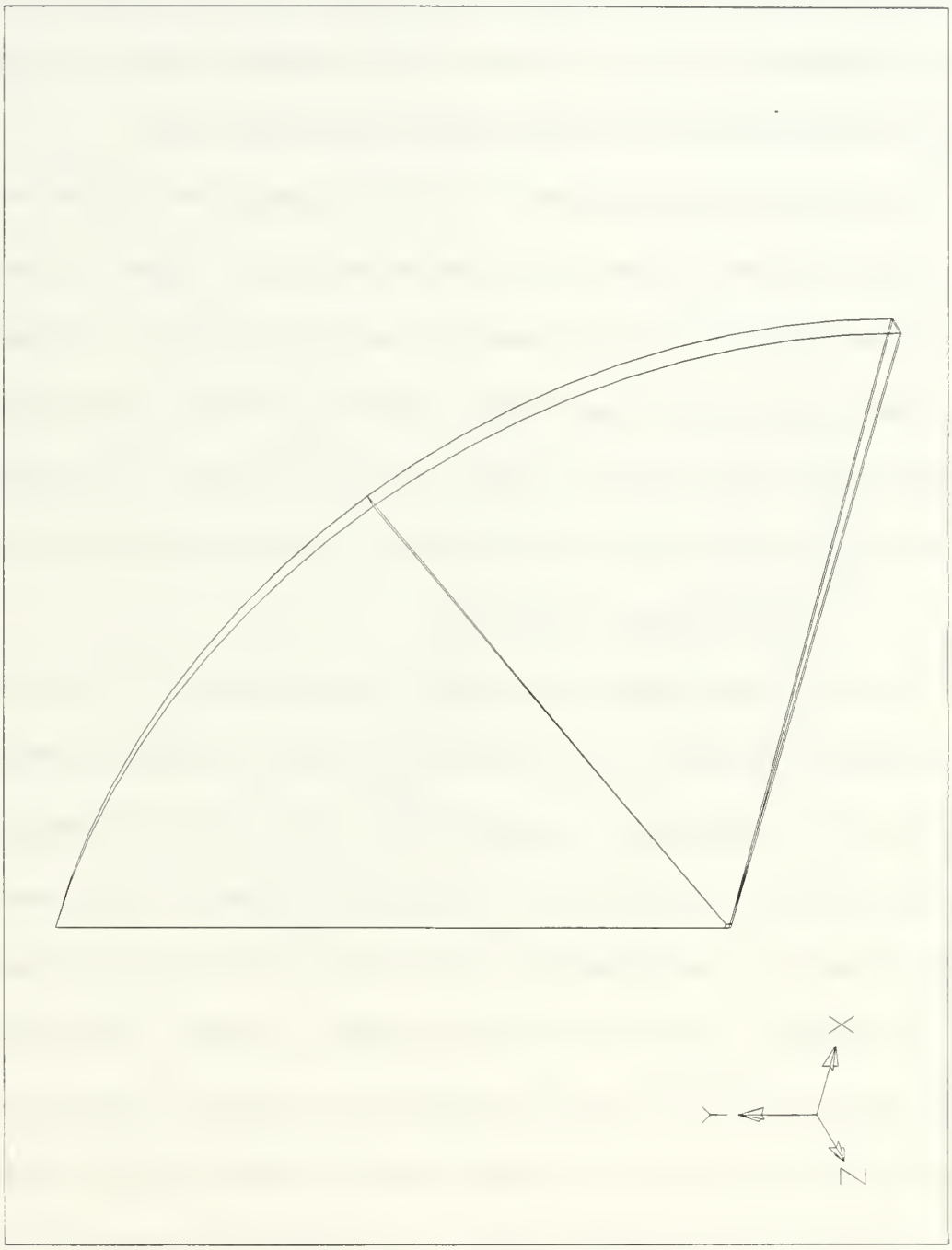

Figure 4-6. Overall Model Geometry for h*=1.380 Analyses

dimensional perspective. This figure is for the analyses in which h^* has a value of 1.380. Figure 4-7 shows an expanded view of the geometry of this model, near the central region. In these figures, the lower of the triangular shaped areas parallel to the z-x plane is the rigid wall or constant pressure boundary. The upper (interior) triangular shaped area bisects the center of the charge, and was the symmetry plane for the free-field analysis.

The overall finite volume mesh used for the model geometry shown in Figures 4-6 and 4-7 is shown in Figure 4-8, from a two-dimensional perspective. Figure 4-9 shows an expanded two-dimensional view of this model in the region near the charge. As in the free-field model, this model has a square meshed central region, which for this model is a rectangular wedge 247.5 cm wide by 345 cm high. This is bordered on two sides by a transition region connecting this square meshed area with the more coarsely meshed outer region.

The lower boundary parallel to the z-x plane in Figures 4-6 through 4-9 is made either a rigid boundary or a constant pressure boundary, by imposition of boundary conditions on the faces of the elements which lie on this boundary. For the rigid wall analysis, the appropriate boundary condition is a "no-flow" condition. For the constant pressure boundary analysis, the pressure on the element faces which constitute this boundary is made equal to the initial hydrostatic pressure in the surrounding fluid, for all time. The other flow parameters (velocity, density, and specific internal energy) at the boundary then take on the values in the finite volumes in to or out of which material is flowing. This constant pressure boundary is only an approximation of an actual air-water interface, as it does not account for changes in the shape of the boundary (which is assumed to remain planar).

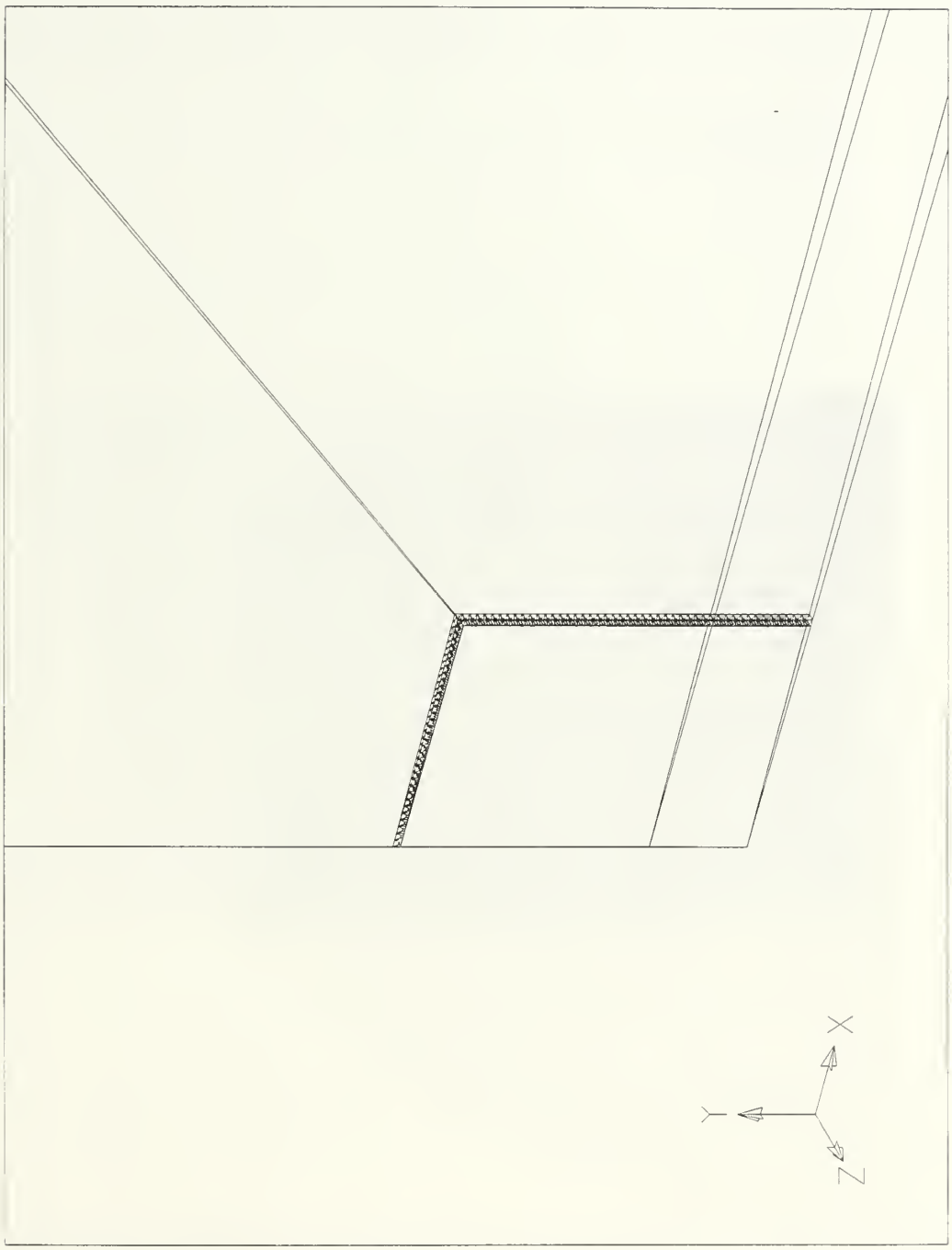

Figure 4-7. Model Geometry for h*=1.380 Analyses in Area Near Charge

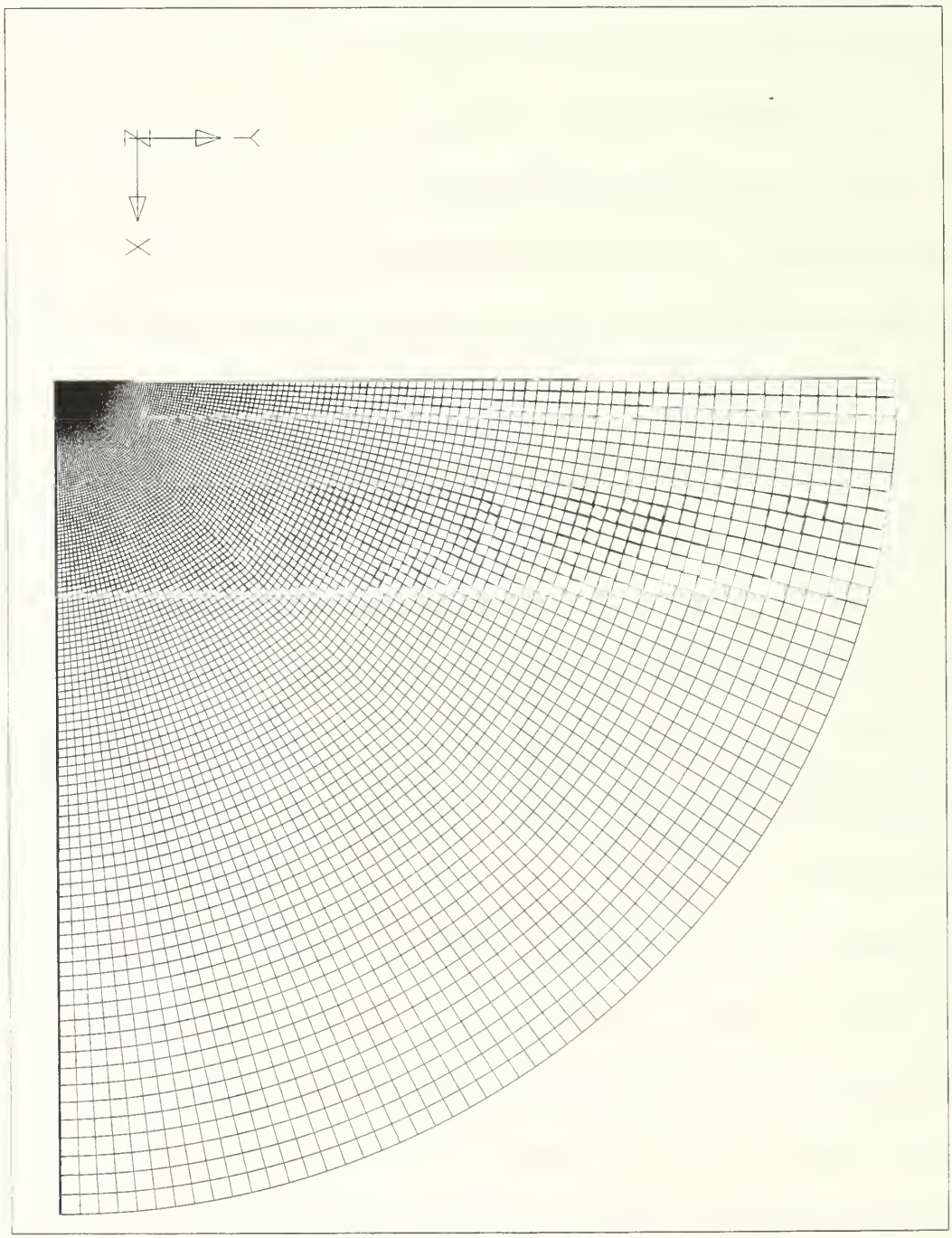

Figure 4-8. Overall Finite Volume Analysis Mesh for h*=1.380 Analyses

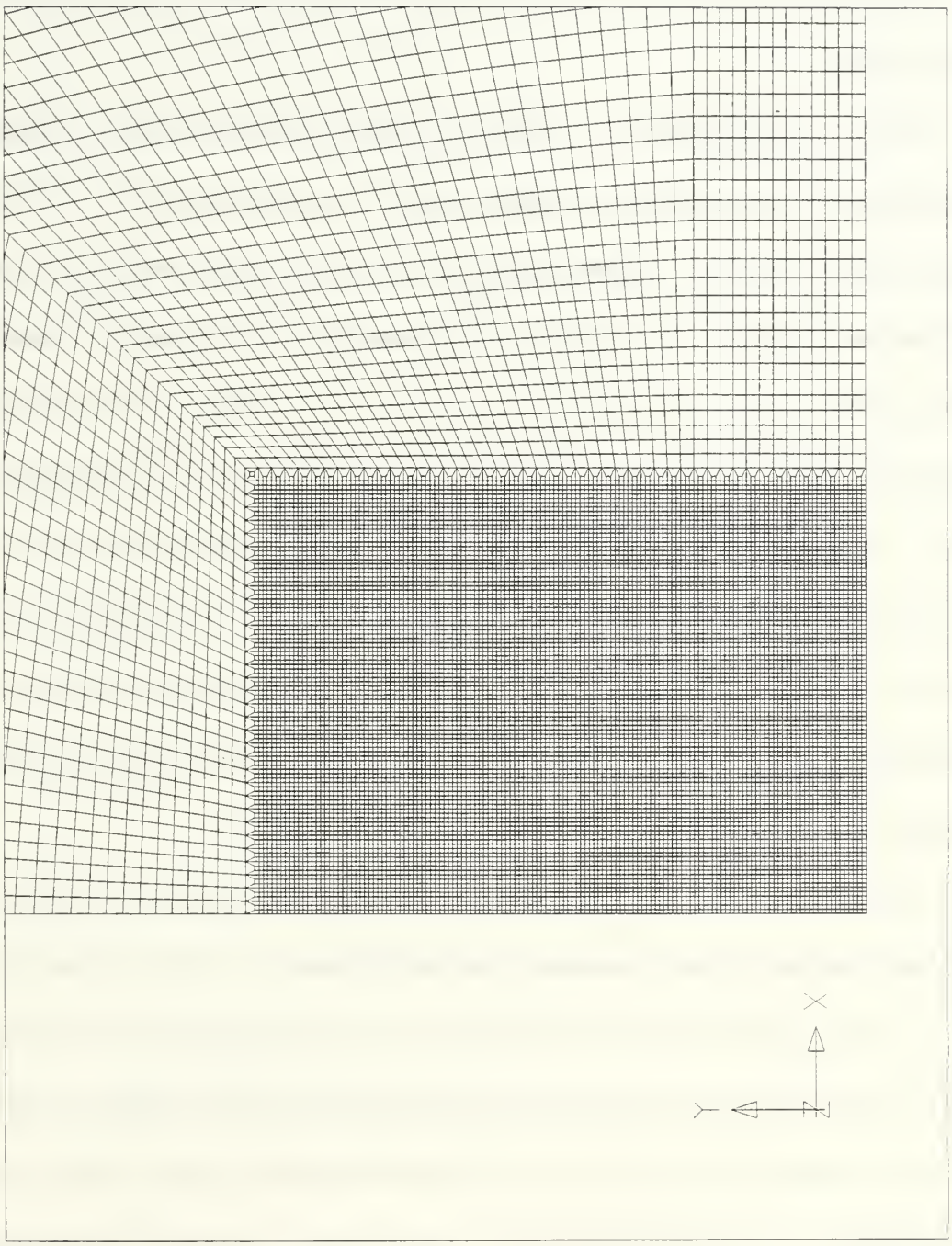

Figure 4-9. Finite Volume Analysis Mesh for h*=1.380 Analyses in Area Near Charge

The finite volume models for the other analyses conducted at various other standoff distances are very similar to the model shown in Figures 4-6 through 4-9. These models vary only in the amount of fluid added between the plane bisecting the axis of the charge and the boundary plane.

The 10.24 kg cylindrical TNT charge used in the simulations discussed in this chapter is modeled as a 20 cm high, 20 cm diameter charge with an initial density of 1.630 g/cm^3. Properties for this charge were modeled using a JWL form state equation, with state equation parameters taken from the *Lawrence Livermore National Laboratory Explosives Handbook* (Dobratz, 1981). This is the same state equation described in Chapter III, and the same parameters given there for this state equation were used for the analyses described in this chapter. In Figures 4-8 and 4-9, all of the elements initially contain seawater, with the exception of the 32 elements initially containing the TNT charge. This charge is shown as shaded elements in Figure 4-10. This TNT is detonated using a spherical detonation wave traveling outward from the center of the charge (midway up the charge on the axisymmetric symmetry axis) at a constant velocity of 6930 m/s.

The seawater in all of the remaining elements was modeled using the same polynomial state equation and state equation parameters described in Chapter III. Initial conditions in this seawater were an initial density of 1.025 g/cm^3, and an initial pressure of 10.153 MPa (0.10153 Kbar), which is the total hydrostatic pressure (atmospheric plus seawater head). As discussed in Chapter III, this initial pressure was set by specifying a nonzero initial specific internal energy (20076 J/Kg) to avoid round off errors (even at a depth of 1000 m, there is only a minuscule density increase). Using a constant volume specific heat value of about 1

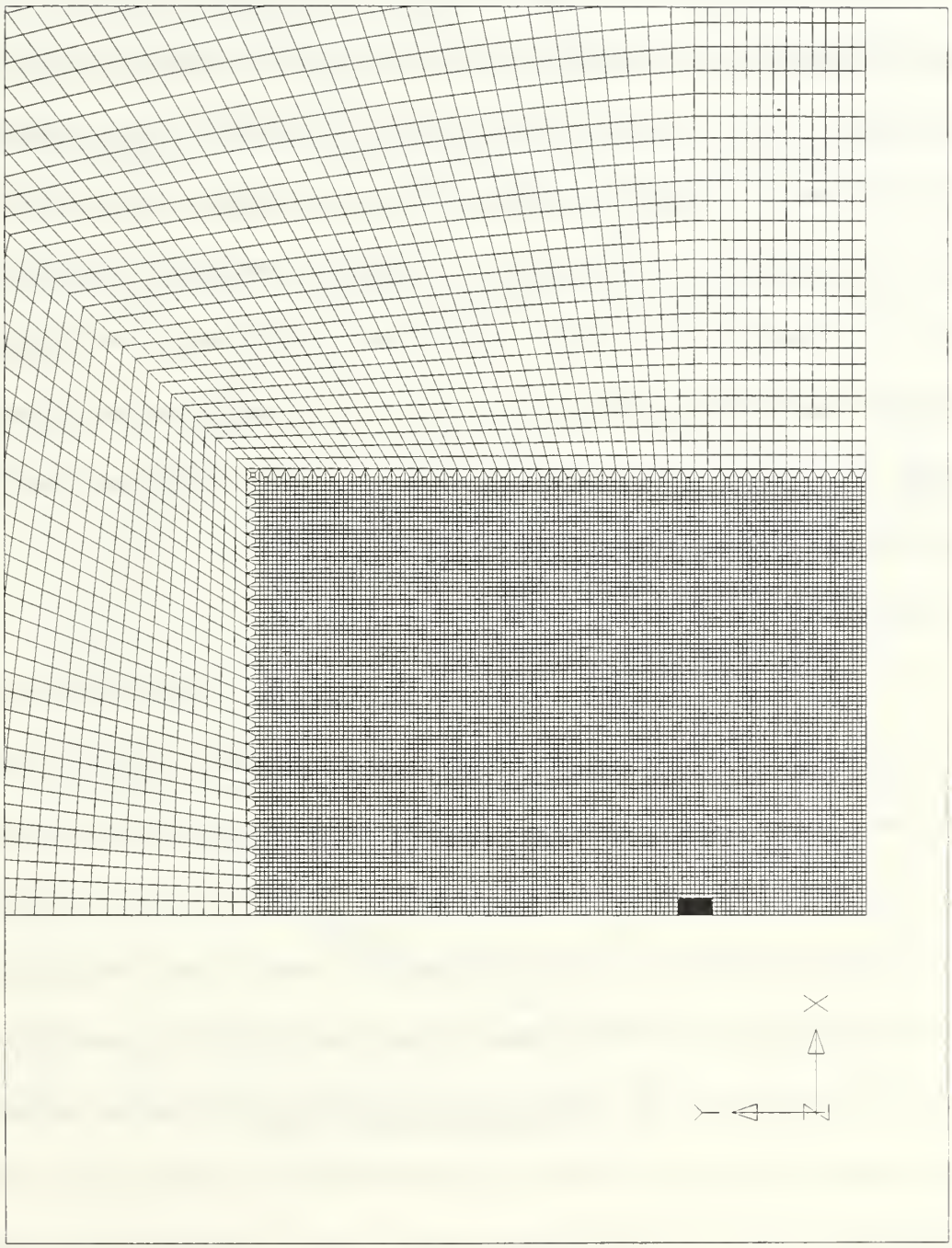

Figure 4-10. Locate of Charge in Finite Volume Analysis Mesh for h*=1.380 Analyses

cal/g C, this works out to a temperature change of only 7.8 C, for which the results should not be affected.

Several simplifying assumptions were made in these numerical analyses. As in the simulation described in the last chapter, the seawater was assumed to behave as an invicid and irrotational fluid. Heat and mass transfer between the seawater and the explosion gas bubble were also assumed to be negligible over the time frame of the analyses. Herring (1950) has shown the peak stresses due to viscosity are negligible in comparison with hydrostatic pressure, even using Taylor's (1943) velocity field (which is known to significantly overestimate the bubble migration velocity), and that the transfer of heat over one bubble oscillation cycle through conduction at the surface of the bubble constitutes a negligible fraction of the total energy of the explosion.

C. SIMULATION RESULTS

1. The Effect of Boundaries on Bubble Period in a Compressible Fluid

As discussed in the introduction, the period of the first bubble oscillation and the displacement of the bubble during this time interval are important factors in determining the amount of damage that the bubble can cause. Figure 4-11 shows the volume equivalent spherical radius (the radius of a spherical bubble with the same volume) time history, for analyses in which a rigid and a constant pressure boundary were located at a standoff distance of 1.380 maximum free-field radii. The use of the volume equivalent spherical radius as the ordinate scale in this figure is not meant to imply that bubbles were actually spherical when a boundary was present. This ordinate scale is simply $(3V/4\pi)^{1/3}$, and was chosen merely for convenience in comparing results from the various analyses with the free-field analysis results.

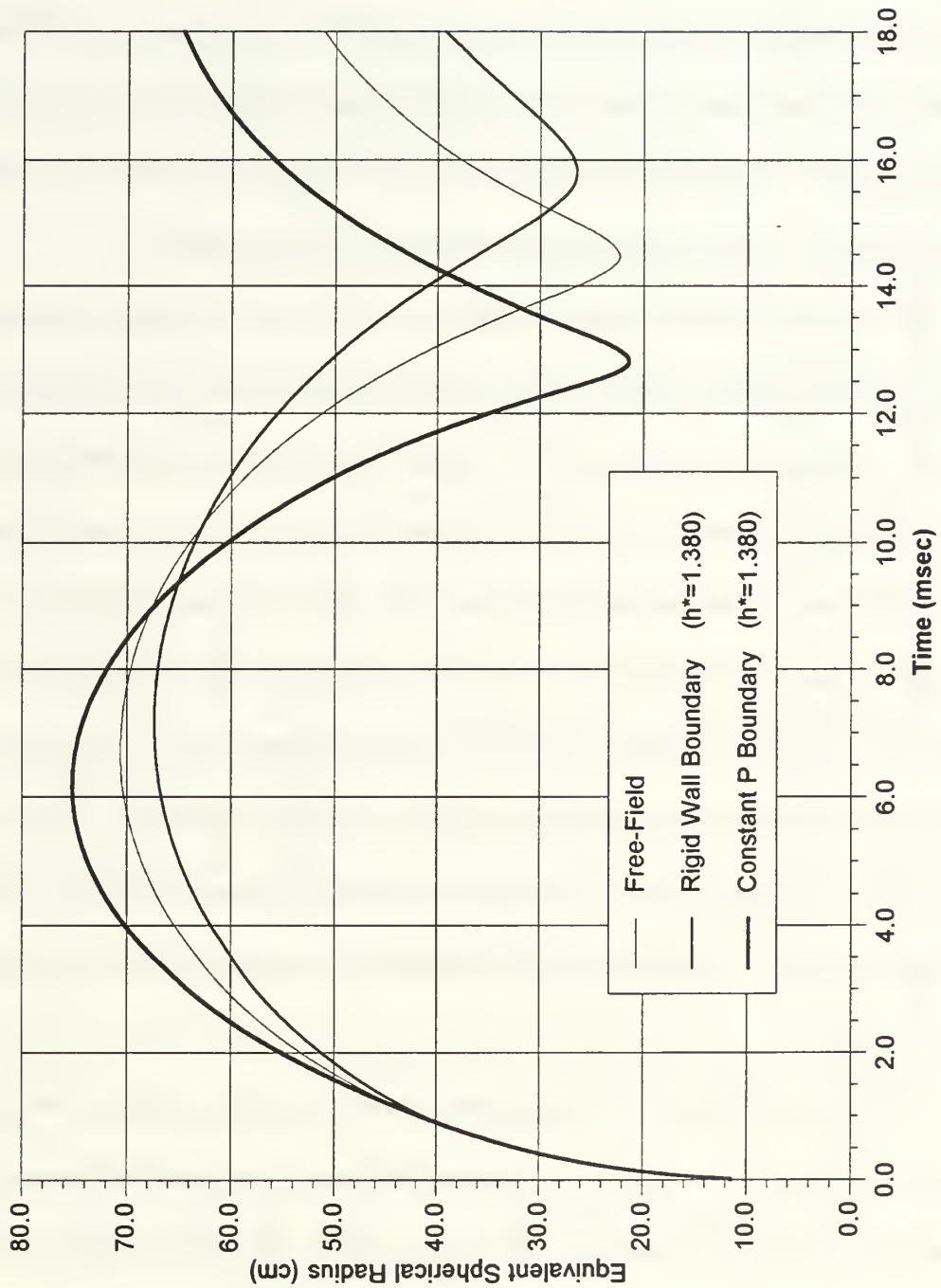

Figure 4-11. Bubble Radius Time History for Free-Field and h*=1.380 Analyses

The free-field radius-time history is also shown in this graph for comparison purposes. The period of the bubble is obviously influenced appreciably by the presence of the nearby boundary, as is the maximum volume of the bubble. Similar bubble volume equivalent radius time history data was generated for the analyses conducted at the other initial standoff distances, and used to determine the individual bubble oscillation periods.

By compiling the bubble period results from the numerical analyses conducted at different standoff distances, the effect of the standoff distance to each type of boundary can be assessed. This is done in Figure 4-12, in which the non-dimensional bubble period T^* (where T^* is the first bubble period in units of free-field bubble periods) is plotted against the *inverse* of the non-dimensional standoff distance h^*. For convenience, the results from analyses with rigid wall boundaries are shown on the same graph with results from analyses with constant pressure boundaries. The inverse standoff distance with an ordinate value of 0.0 represents the situation in which the boundary is located at infinity (i.e. the free-field case). Points to the right of this represent non-dimensional inverse standoff distances to a rigid wall, and points to the left are non-dimensional inverse standoff distances to a constant pressure boundary.

Also plotted in Figure 4-12, for comparison purposes, is the non-dimensional period versus the inverse of the non-dimensional standoff distance (T^* vsersus ($1/h^*$)) relationship predicted by an approximate analysis due to Herring (1950). In Herring's analysis, the fluid is assumed to be incompressible, the gas bubble is assumed to have negligible internal energy and remain nearly spherical, and the bubble is assumed to be fairly remote from the boundary (terms of order $1/h^{*2}$ and higher are neglected). Herring's formula for the bubble period can

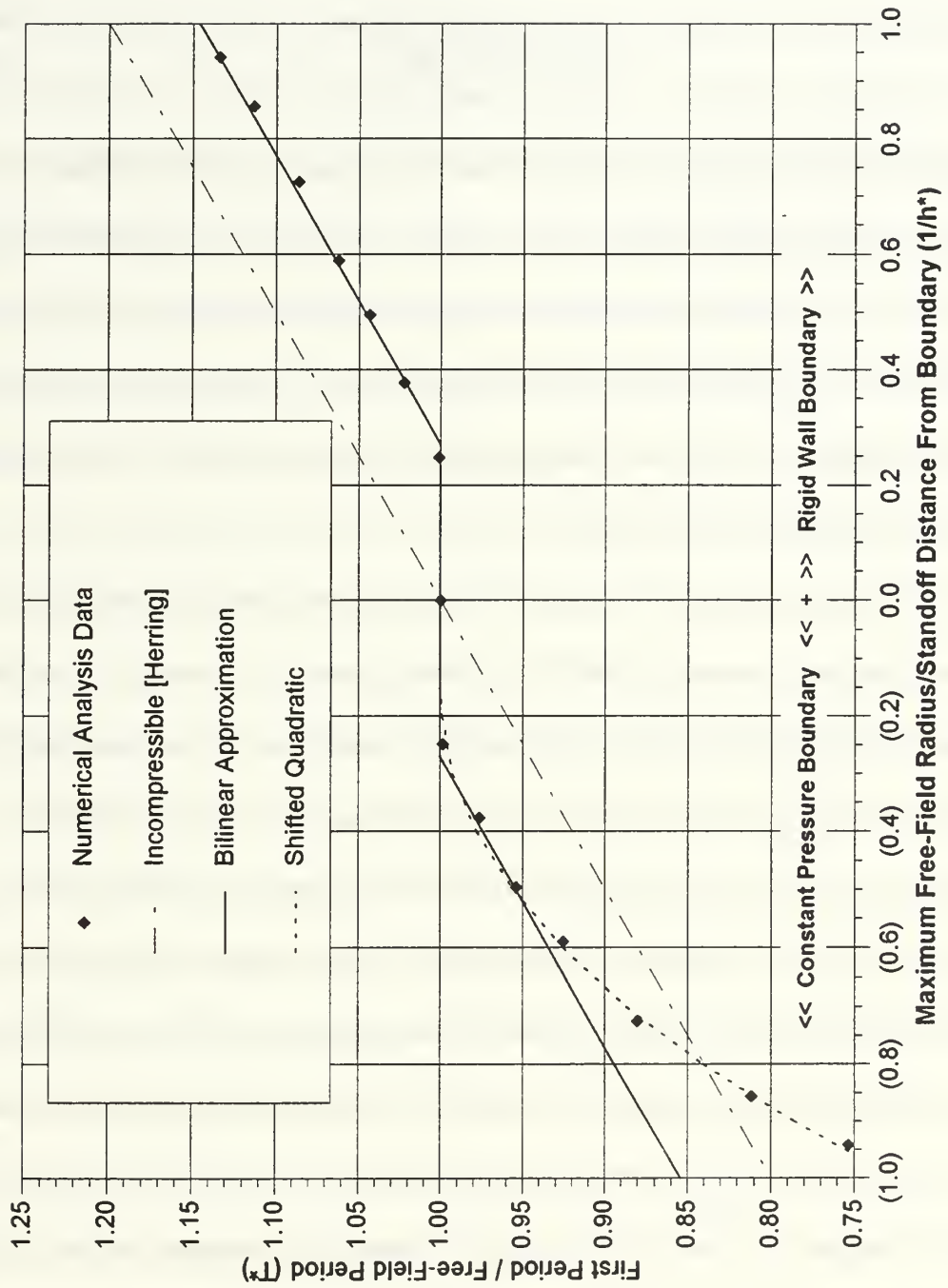

Figure 4-12. Bubble Period Variation with Standoff Distance to Rigid and Constant Pressure Boundaries

be expressed as

$$T^* = \left(1 \pm \frac{(R_{ave}/R_{max})}{4h^*} \right) \tag{4-1}$$

where R_{ave} is the average radius of the free-field bubble during the first oscillation, and R_{max} is the maximum free-field radius. In this equation, the upper (plus) sign is for a rigid wall boundary, and the lower (minus) sign is for a constant pressure boundary. The R_{ave} value is determined by integrating the free-field radius vs time curve over the first period, and then dividing by that period; here, the free-field radius vs time curve from the numerical analysis was used, and integrated numerically.

It is interesting that the T^* versus $1/h^*$ curve generated from the numerical analyses has about the same slope as that predicted by Herring's analysis, for the rigid boundary type. Herring's analysis neglected terms of order $(1/h^{*2})$ and higher, and assumed small bubble shape deviations from spherical, so it is apparent that equation (4-1) could be in error for charges fairly near a boundary surface. Since Herring neglected compressibility of the surrounding fluid, and changes in the surrounding flow field caused by passage of the initial shock wave (which, as seen in the results in the last chapter, can extend over an appreciable distance from the bubble), equation (4-1) can also be shown to be in error for charges very remote from a boundary. In a compressible fluid, there is a finite standoff distance beyond which the absence or presence of a boundary can have no affect upon the first oscillation period of the bubble, owing to the finite wave speed in a compressible medium. Thus, in Figure 4-12, for a compressible fluid there must exist a finite region of abscissa values on either side of the 0.0 $1/h^*$ value for which T^* must be equal to 1.0. This distance can be

estimated, assuming a constant wave speed of about 1500 m/s in seawater, as half the distance traveled by shock wave in 14.47 msec (the free-field bubble period), i.e. about 10.85 meters. This corresponds to an h^* value of about 15.4 (and a $1/h^*$ value of about 0.065). Furthermore, if the boundary is located somewhat closer it should have still have little effect upon the bubble period, as most of the oscillation of the bubble will have already occurred before the reflection of the primary shock wave gets back to the bubble.

Thus, although equation (4-1) is the classical correction for the effect of rigid boundaries and free-surfaces on the oscillation period of an explosion gas bubble, a better correction can be made by including fluid compressibility. One question that arises is how the results from this investigation this might be applied underwater explosion gas bubbles resulting from other charge types, weights, and depths. One solution is to use a simplified fit through the data points in Figure 4-12. One proposed fit is a "bilinear" one through the data points for either type of boundary. The term "bilinear" is meant to imply that, for either a rigid wall or a constant pressure boundary individually, the curve consists of two linear segments (one of which has zero slope). This proposed fit is shown as a solid line in Figure 4-12, and labeled as a "Bilinear Approximation." One limitation of this fit is that its accuracy decreases rapidly for standoff distances of less than two maximum free-field radii, for the constant pressure type of boundary (i.e. for $1/h^*$ values greater than 0.5). For the rigid wall type of boundary, it appears to be reasonably accurate over the entire range of standoff distances shown in Figure 4-12.

The advantage of this bilinear approximation lies in the relative ease with which it can be utilized for other charge type, weight, and depth parameters, as will be discussed shortly.

The functional form for this proposed period correction factor for the effect of a boundary surface on the first period of an explosion gas bubble is given by the expression

$$T^* = 1 \pm u\left(\frac{1}{h_T^*}\right)\frac{R_{ave}/R_{max}}{4h_T^*} \tag{4-2}$$

where u is a unit step function (zero if its argument is negative, one if its argument is positive), R_{ave} is the average free-field bubble radius over the first period, R_{max} is the maximum free-field bubble radius, and h_T^* is *defined* by

$$\frac{1}{h_T^*} = \frac{1}{h^*} - \frac{1}{h_0^*} \tag{4-3}$$

where h_0* is an effective maximum standoff distance (in units of maximum free-field radii) for which the period of the bubble starts to be effected appreciably by the presence of a boundary surface. In Figure 4-12, this is the point at which the slope of the bilinear approximation curve changes from 0.00 to 0.20. For the bilinear approximation curve shown in Figure 4-12, this effective maximum standoff distance is given by $1/h_0^* = 0.27$, i.e. h_0* has a value of about 3.7 maximum free-field radii.

In order to apply Herring's correction factor, equation (4-1), it was necessary to know the quantity R_{ave}. This implies knowledge of the free-field radius time history curve, but since the *shape* of this curve varies little with the particular explosion parameters, the value of R_{ave} will generally be close to 0.8 R_{max}. To apply equation (4-2), it is necessary to know, in addition, the value of the parameter h_0*. In general, this parameter may be a function of the

charge type, weight, and depth. However, it should be relatively easy to determine an empirical expression for this parameter for different types of explosives, since for a particular charge weight and depth, this parameter can be determined by a single accurate measurement of how much Herring's correction factor is in error for a single (well chosen) standoff distance.

An example should clarify this. Suppose that an experiment were conducted using a particular charge type, weight, and depth, at a standoff distance of h^*=2.00 from a rigid boundary, and Herring's correction factor was determined to predict a period increase of 10%. The value of R_{ave}/R_{max} is then 0.8, from equation (4-1). If the actual period increase for this experiment was measured to be 4.6%, then, from equation (4-2), $1/h_T^*$=0.23. Thus, from equation (4-3), $1/h_0^*$ = 0.27.

Again, the range of validity of equation (4-2) should be kept in mind. From Figure 4-12, an appropriate limitation would appear to be h^*>2.0 for a constant pressure boundary, and h^*>1.0 for a rigid boundary.

For calculation of the first bubble period at standoff distances less than two maximum free field bubble radii from a constant pressure boundary, a better approximation is needed. A "Shifted Quadratic" fit for the constant pressure boundary data shown in Figure 4-12 is defined by

$$T^* = 1 - u\left(\frac{1}{h_{TCP}^*}\right)\frac{m_{TCP}}{(h_{TCP}^*)^2} \qquad (4\text{-}4)$$

where u is a unit step function and

$$\frac{1}{h^*_{TCP}} = \frac{1}{h^*} - \frac{1}{h^*_{0CP}} \qquad (4\text{-}5)$$

This characterization depends upon two parameters. The fit shown did not require a linear term in the shifted non-dimensional inverse standoff distance. The values for the shifted quadratic fit shown in Figure 4-12 fitting the numerical analysis data were m_{TCP}=0.4 and h^*_{0CP}=0.17. The range of validity for the fit defined by equations (4-4) and (4-5) is h^*>1, i.e. it is valid for any standoff distance from a constant pressure boundary. The fact that the non-dimensional period change seems to vary linearly with the non-dimensional inverse standoff distance for a rigid wall boundary and as the square of the non-dimensional inverse standoff distance for a constant pressure boundary may well have some physical cause or explanation.

2. The Effect of Boundaries on Bubble Migration in a Compressible Fluid

The bubble center of mass displacement time history for the analyses in which a rigid boundary and a constant pressure boundary were located at an initial non-dimensional standoff distance of h*=1.380 is shown in Figure 4-13. This is the same case for which the bubble volume equivalent radius time history curves were shown in Figure 4-11. In Figure 4-13, the displacement is taken to be positive if it is towards the boundary, and negative if it is away from the boundary. For the rigid wall boundary analysis, this figure shows a small initial migration of the bubble away from the boundary at early times (when the bubble is expanding). At later times (when the bubble is contracting) there is a significant migration towards the boundary. This migration is much larger than the initial migration away from the boundary, and the rate of migration increases as the bubble contracts to its minimum volume.

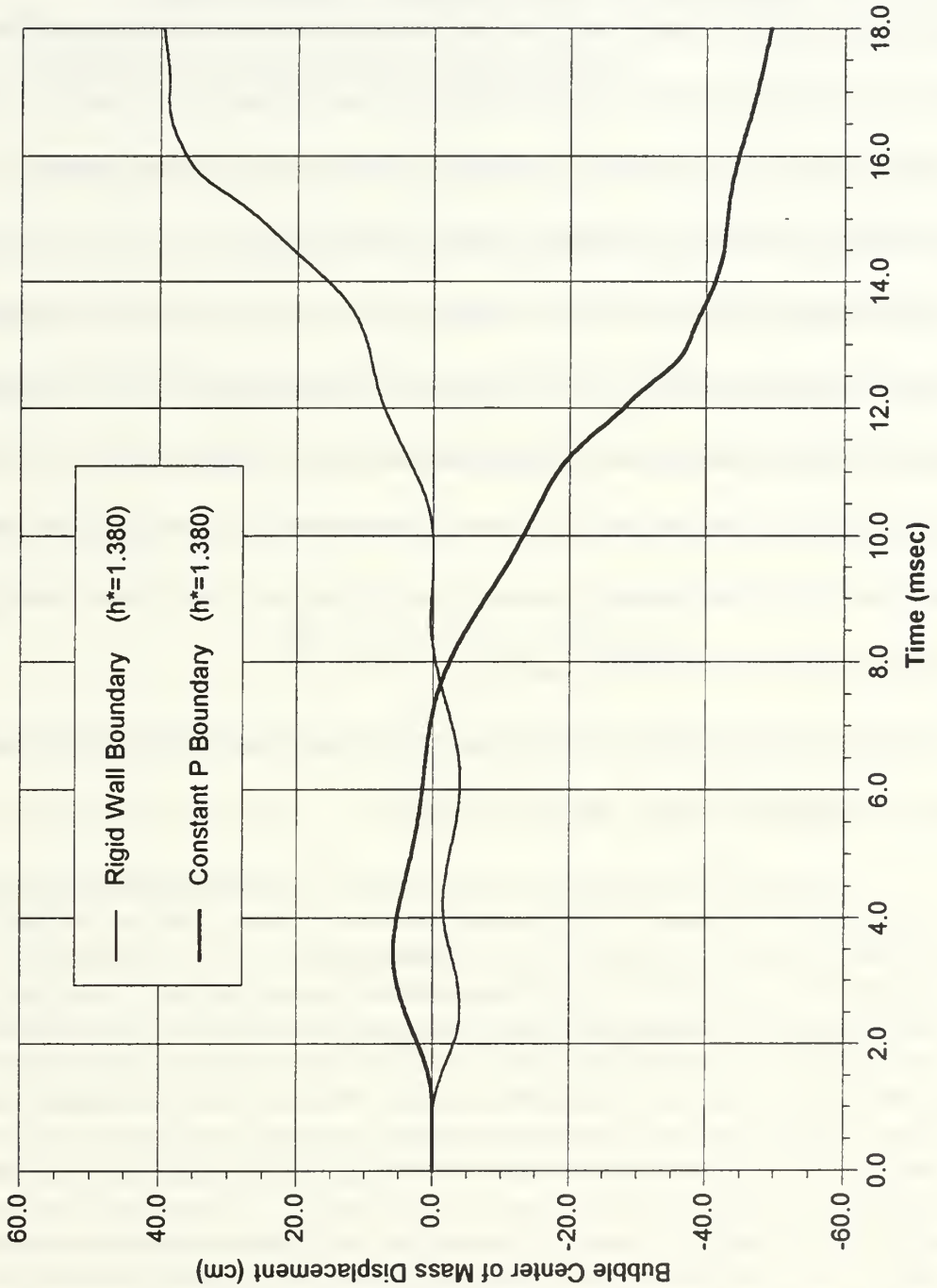

Figure 4-13. Bubble Center of Mass Displacement Time History for h*=1.380 Analyses

The opposite affect is seen when the boundary is a constant pressure boundary; the bubble initially moves towards the boundary, and later moves rapidly away from the boundary. The influence of fluid compressibility is also seen in Figures 4-11 and 4-13. There is an initial interval of time during which neither the type nor even the presence of the boundary affects the volume of the bubble, and it is not migrating.

The displacement time histories, whose overall characteristic is described above, also show a small amplitude higher frequency component. The period of this small amplitude component is about twice the time interval between the start of the analyses and the time when the bubble begins migrating, which seems to be roughly proportional to the standoff distance. Hence, this higher frequency component would appear to result from the reflection of the primary shock wave from the boundary.

The general shape of the bubble displacement curves, as seen in Figure 4-13, has been qualitatively explained by Cole (1948, pp. 331-332):

> In the case of a rigid surface, the presence of the boundary interferes with radial fluid flow of water, whether outward or inward, near a spherical surface in its vicinity. Initially, when the pressure in the gas is in excess of the hydrostatic pressure, the water on the side of the bubble surface near the wall is less readily displaced, and the bubble surface moves away from the wall. The effect is relatively small, however, because the net pressure (in excess of hydrostatic) is positive for a short part of the bubble period, and the bubble is small during this time. When the pressure falls below hydrostatic, acceleration of flow toward the bubble surface does not occur as readily on the side toward the wall, and the flow must be such as to bring the surface nearer to the wall. A considerable amount of momentum is imparted to a large mass of water in this way when the bubble is large. As the bubble contracts, the momentum acquired becomes concentrated in a smaller mass of water near the bubble, and the velocity of flow in this region increases. The bubble surface must then move toward the wall with increasing speed as if attracted to it. This effect is so much larger than the repulsion when the pressure exceeds hydrostatic that the dominant motion is an apparent attraction increasing the bubble velocity toward the wall as it contracts, even

though the momentum of the flow is decreasing in the most contracted stages.

A free surface has the opposite effect on bubble migration, as in this case the water at the surface is free to move but must due so in such a way as to equalize the pressure with that of the atmosphere.

Herring (1950) conducted an approximate analysis for the migration of bubbles near plane rigid and free surfaces, in which the method of images is employed for motion of a bubble in an incompressible fluid, the internal energy of the bubble is neglected, the bubble is assumed to be not too near the boundary surface (terms of order $1/h^{*2}$ and higher are neglected) and remain nearly spherical, and migration of the bubble is treated as a small correction to the motion of the bubble. Herring's formula for the migration velocity of the center of the bubble is

$$\pm\frac{dh}{dt}=\frac{3r^2}{4h^2}\frac{dr}{dt}-\frac{3}{2h^2r^3}\int_0^t r^4\left(\frac{dr}{d\tau}\right)^2 d\tau \qquad (4\text{-}6)$$

where t is the time, h is the standoff distance between the boundary and the center of the bubble, and r is the radius of the bubble. In this equation the plus sign is for a rigid boundary, and the minus sign is for a free surface.

Together with a knowledge of the function $r(t)$, equation (4-6) can be separated and integrated to give an equation for the displacement of the center of the bubble. However, results obtained from doing so are known to be in poor agreement with experimental results, significantly over predicting the migration of the bubble late in the collapse phase (Cole, 1948, p.348). This is when the assumptions used by Herring in his analysis are least accurate, as the migration of the bubble at this time is not a small perturbation of the free-field bubble motion, and the time rate of change of the bubble radius is over predicted if internal energy is neglected.

Nevertheless, it is worth noting that the first term on the right hand side of equation (4-6)

is a periodic term which changes sign when *dr/dt* changes sign, i.e. when the bubble is at its maximum radius. The second term is monotonic, and builds up to a large value when the magnitude of *dr/dt* becomes large. This is in qualitative agreement with the behavior seen in the displacement versus time results for the various numerical analyses.

As discussed earlier, the location of an explosion gas bubble at the end of its first oscillation is important because this is where the bubble pulse originates from. Taking a cue from Figure 4-12, values for the bubble displacement at the time the bubble reached minimum volume (which varies depending upon the boundary type and initial standoff distance) were compiled for the different numerical analyses, and plotted as a function of the *inverse* standoff distance. This plot is shown in Figure 4-14, in which the abscissa values represent the non-dimensional inverse standoff distance, with values to the right of 0.0 being for a rigid boundary and values to the left of this point being for a constant pressure surface, as in Figure 4-12. The total displacements at the time of the first minimum is plotted in units of maximum free-field radii, so that a value of 0.4, for example, represents a center of mass displacement of 0.4*70.65 cm from the initial center of the charge.

The effect of a finite wave speed in a compressible fluid is again seen in Figure 4-14; remote boundaries cause little or no displacement of the bubble. This plot shows a general linearity for bubbles fairly near either type of boundary. The only exception is the case in which the bubble was initially closest to a constant pressure boundary, for which the initial migration towards the boundary and the increase in the bubble radius over the free-field value cause the bubble to actually contact the boundary when the bubble was near maximum radius. Neglecting this left most point in Figure 4-14, the results show that the first period displacement near either

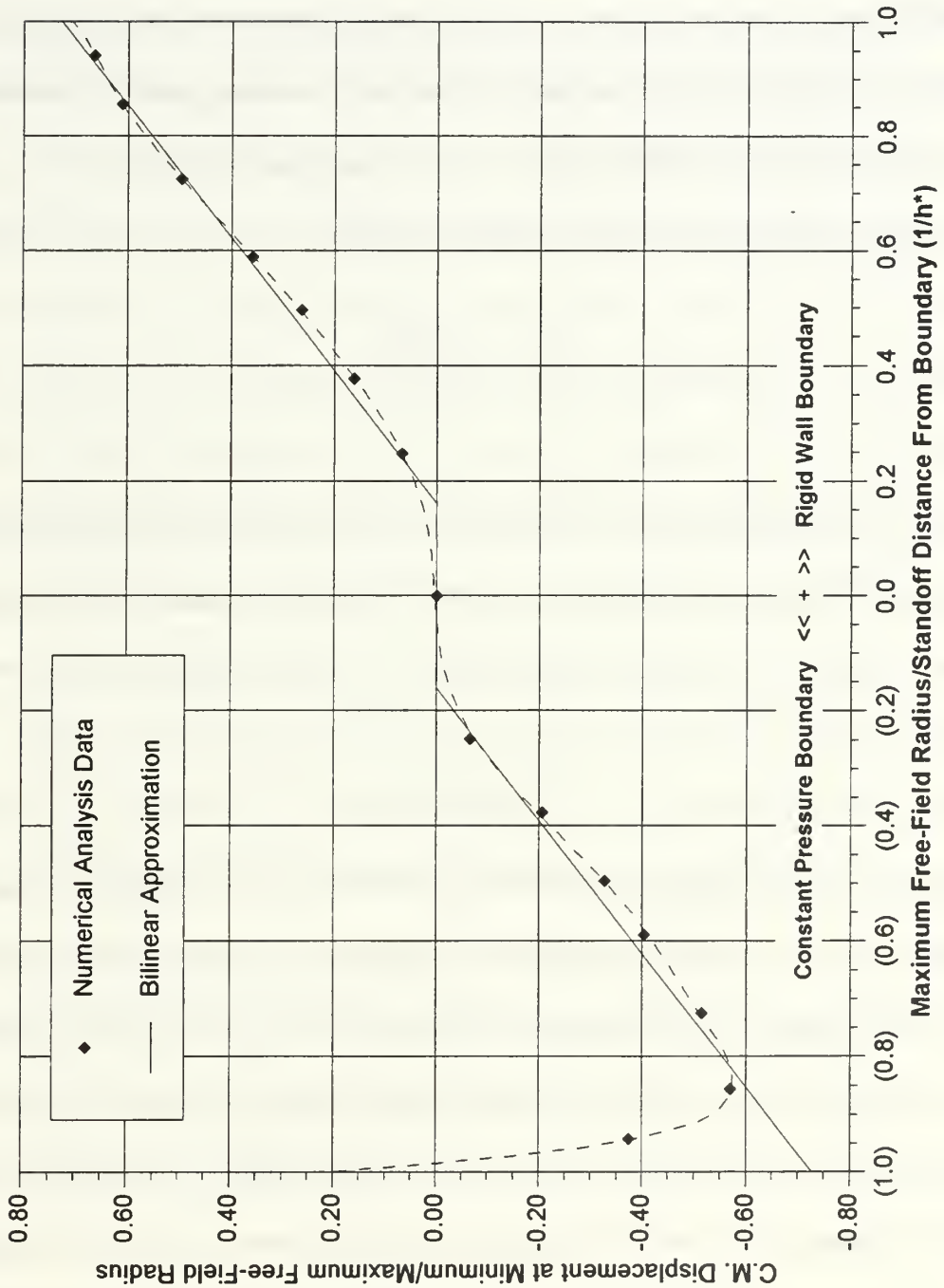

Figure 4-14. Bubble C.M. Displacement at First Minimum Variation with Standoff Distance to Rigid and Constant Pressure Boundaries

type of surface can be well approximated by a bilinear curve when plotted against the inverse standoff distance. This curve is shown as a dashed line in Figure 4-14. The slope of the non-zero portion of this curve is about the same for either type of boundary, again suggesting a general semi-empirical formula for bubble migration near either type of boundary.

The proposed functional form for this formula is

$$\Delta Y^* = u\left(\frac{1}{h_Y^*}\right)\frac{m_Y}{h_Y^*} \tag{4-7}$$

where ΔY^* is the displacement at the first minimum in free-field radii, u is a unit step function, m_Y is the slope of the non-zero slope portion of the "bilinear approximation" curve, as shown in Figure 4-14, and h_Y^* is a effective standoff distance for bubble migration, given by

$$\frac{1}{h_Y^*} = \frac{1}{h^*} - \frac{1}{h_1^*} \tag{4-8}$$

where h^* is the actual standoff distance in maximum free-field bubble radii, and h_1^* characterizes a maximum effective standoff distance for which appreciable bubble migration occurs.

For the bilinear approximation curve shown in Figure 4-14, m_Y and h_1^* have the values of about 0.87 and 6.2, respectively. Again, these parameters might vary with charge type, weight, and depth, but can be determined empirically without great difficulty. The proposed bilinear fit given by equations (4-7) and (4-8) appears, from Figure 4-14, to be a reasonably good approximation for total bubble migration at the time of the first minimum for standoff distance values $h^*>1.25$ for the constant pressure type boundary, and $h^*>1$ for the rigid wall type boundary.

3. Bubble Shape Departure From Spherical

While the time at which the bubble reaches its minimum volume and the displacement of the bubble at this time, and the effect of standoff distance on these quantities, were the primary items of interest in these analyses, the overall shape variation of an explosion gas bubble generated near a boundary surface is also of interest. In approximate analytical derivations such as for equation (4-1), the bubble is assumed to remain nearly spherical. It is of some interest to see how nearly true this assumption is, if only to form some opinion as to the validity of the derivation. While the analysis code used in these numerical analyses does not actually keep track of the location of the boundary surface between different materials within the mesh, it is possible to get an overall view of the shape of the bubble by examining the density of the various mesh volumes.

Figure 4-15 shows the results for the analysis case in which a plane constant pressure boundary was initially located at a standoff distance of 1.380 maximum free-field radii from the center of the charge. In this figure the dark areas represent the bubble, and the times are given in terms of the first period of the bubble. The boundary plane is that plane below which times are indicated. The bubble is seen to be fairly spherical when near its maximum volume, but to have a pronounced "kidney shape" by time 80% of its first oscillation period has elapsed. It then continues deforming, eventually assuming a "spherical cap" shape by the time it reaches minimum volume. This figure also shows the migration of the center of mass of the bubble away from the boundary.

Figure 4-16 shows the variation of the bubble shape with time when a rigid boundary was located at 1.380 maximum free-field radii from the center of the charge. Again, the dark area

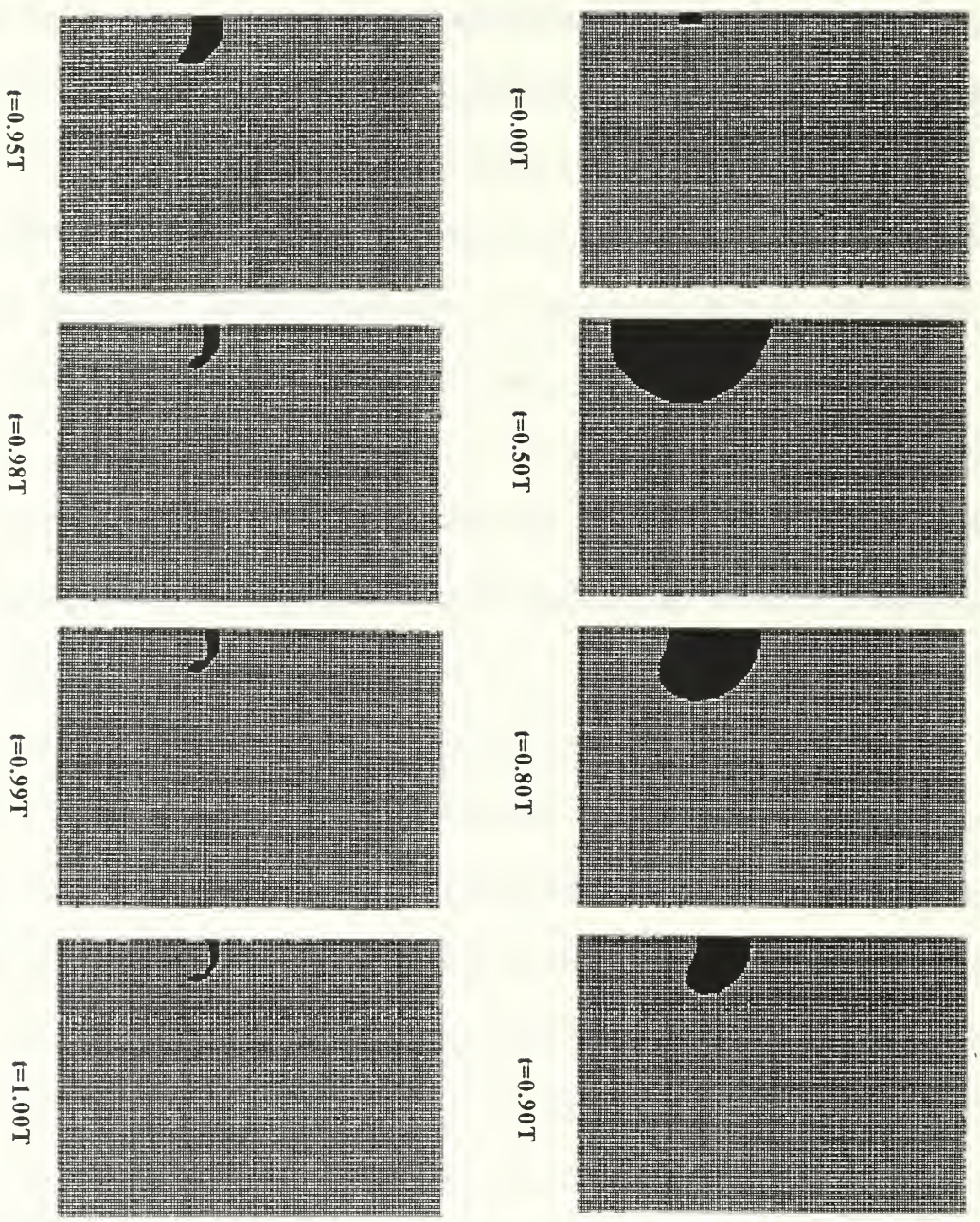

Figure 4-15. Bubble Shape Variation with Time for Bubble Located at h*=1.380 from a Constant Pressure Boundary

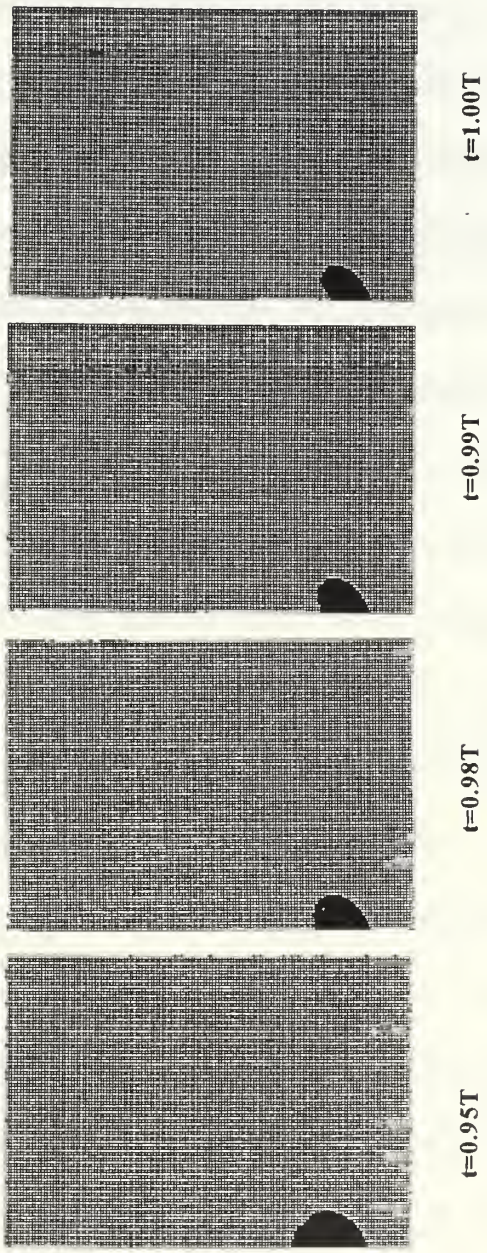

Figure 4-16. Bubble Shape Variation with Time for Bubble Located at h*=1.380 from a Rigid Boundary

represents the bubble, and the boundary plane is that plane below which times are indicated. In this figure, bubble shapes are only shown for the last 5% of the first oscillation period; at 95% of the first bubble oscillation period the bubble is still nearly spherical. By 98% of the first oscillation period, the bubble has become "kidney"-shaped.

From these figures, it might be expected that derivations assuming bubble sphericity would be better at this standoff distance for the rigid boundary case than for the constant pressure boundary case. Examining the bilinear approximation in Figure 4-12, which can be thought of as a compressibility corrected approximation to Herring's derivation of equation (4-1), this would seem to be the case.

V. CONCLUSION

The current understanding of the effects of fluid compressibility on the dynamic behavior of underwater explosion gas bubbles is very limited; the existing theories for underwater explosion gas bubble phenomena neglect entirely the effects of fluid compressibility. As a consequence, these theories fail to accurately predict important phenomena associated underwater explosion gas bubbles. It was for this reason that the research described in this dissertation was undertaken.

In the first part of this investigation, it was shown that a finite volume based numerical analysis technique which incorporated fluid compressibility could accurately account for the behavior of an explosion gas bubble in the free-field case up until the time of the first bubble minimum, and it was verified that the radiation of energy in the bubble pulses does not account for all of the energy loss that occurs between bubble oscillation cycles.

In the second part of this investigation, the behavior of underwater explosion gas bubbles near rigid and constant pressure boundary surfaces was investigated, including effects arising because of fluid compressibility. The failure to account for fluid compressibility in the current theoretical development has made predictions for bubble behavior based upon this theory more qualitatively correct than quantitatively accurate. It was found possible, when fluid compressibility is taken into account, to quantitatively describe the behavior of explosion gas bubbles quite close to a boundary surface.

By conducting analyses at a number of different standoff distances from these boundaries, it was discovered that first bubble oscillation period and the migration of the bubble at the time

it reached minimum volume could be quantitatively described over all standoff distances of interest when fluid compressibility was taken into account. Functional relationships between standoff distance and the first bubble period and the net bubble migration were developed which have a form very suitable for semi-empirically scaling the results of this investigation to situations involving other charge types, weights, and depths.

It is recommended that a series of carefully designed experiments be conducted to both verify the formulas developed in this investigation and to develop the neccessary empirical constants used in these formulas, so that the effects of boundary surfaces can be better taken into account in the future. These results of this investigation should form a foundation for improving the accuracy of calculations for the whipping response of ships and shipboard equipment due to detonation of nearby mines or torpedoes.

LIST OF REFERENCES

Blake J.R., and Gibson, D.C., "Growth and Collapse of a Vapour Cavity Near a Free Surface," *J.Fluid Mech.*, 111, 1981.

Bryant, A.R., "Photographic Measurements of the Size, Shape, and Movement of the Bubble Produced by 1-oz. Charges of Polar Ammon Gelignite Detonated Underwater at a Depth of 3 Feet," *Underwater Explosion Research : A Compendium of British and American Reports*, Vol. II - The Gas Globe, Office of Naval Research, Department of the Navy, 1950.

Chahine, G.L, Frederick, G.S., Lambrecht, C.J., Mair, H.U, and Harris, G.S., "Spark Generated Bubbles as Laboratory-Scale Models of Underwater Explosions and Their Use for Validation of Simulation Tools," Presented at the 1995 Shock and Vibration Symposium, Boloxi, MS, 1995.

Chertock, G., "The Flexural Response of a Submerged or Floating Body to an Underwater Explosion," David Taylor Model Basin Report C-517, 1952.

Chisum, J.E., and Shin, Y.S., *Multimaterial Eulerian and Coupled Lagrangian-Eulerian Finite Element Analysis of Underwater Shock Problems*, Naval Postgraduate School Technical Report NPS-ME-95-001, Monterey, CA, 1995.

Cole, R. H., *Underwater Explosions*, Princeton University Press, Princeton, NJ, 1948.

Dobratz, B.M., *Lawrence Livermore National Laboratory Explosives Handbook*, UCRL-52991, Livermore, CA , 1981.

Herring, C., "Theory of the Pulsations of the Gas Bubble Produced by an Underwater Explosion," *Underwater Explosion Research : A Compendium of British and American Reports*, Vol. II - The Gas Globe, Office of Naval Research, Department of the Navy, 1950.

Herring, C., "Theory of the Pulsations of the Gas Bubble Produced by an Underwater Explosion," National Defence Research Council Report C4-sr20-010, 1941.

Hicks, A.N., "Effect of Bubble Migration on Explosion-Induced Whipping of Ships," Naval Ship Research and Development Center Report 3301, Department of the Navy, 1970 (b).

Hicks, A.N., "The Whipping Forces Experienced by a Ship Very Close to an Underwater Explosion," Naval Ship Research and Development Center Report 3271, Department of the Navy, 1970 (a).

Hicks, A.N., "MSWHIP - An Improved Computer Program to Calculate the Elastic Whipping Response of a Ship to an Underwater Explosion Including Bubble Migration," Naval Ship Research and Development Center, 1971.

Lamb, H. *Philos. Mag. 45*, p. 257, 1923.

Office of Naval Research, *Underwater Explosion Research : A Compendium of British and American Reports*, Department of the Navy, 1950.

Ramsauer, C., *Ann. D. Physik 72*, p. 276, 1923.

Rayleigh, Lord, "On the Pressure Developed in a Liquid During the Collapse of a Spherical Void," *Philos. Mag. 34*, pp. 94-98, 1917.

Reynolds, 0., "Experiments Showing the Boiling of Water in an Open Tube at Ordinary Temperatures," British Association for Advance Science Report 564, 1894.

Schmidt, R.M, Holsapple, K.A, Housen, K.R., and Voss, M.E., "Fundamental Research on the Behavior of Underwater Explosion Bubbles and Their Effects on Marine Structures," Boeing Aerospace Co. Report D180-29720-1R, 1987.

Snay, H.G., "Hydrodynamics of Underwater Explosions," *Symposium on Naval Hydrodynamics*, Publication 515, National Academy of Sciences, National Research Council, 1957.

Swift, E. and Decius, J.C., "Measurement of Bubble Pulse Phenomena, III: Radius and Period Studies," *Underwater Explosion Research : A Compendium of British and American Reports*, Vol. II - The Gas Globe, Office of Naval Research, Department of the Navy, 1950.

Taylor, G.I., "Vertical Motion of a Spherical Bubble and the Pressure Surrounding It," Taylor Model Basin Report 510, 1943.

The MacNeal Schwendler Corporation, *MSC/PISCES User's Manual*, Version 30, Los Angles, CA, 1991.

The MacNeal Schwendler Corporation, *MSC/DYTRAN User's Manual*, Version 2.3, Los Angles, CA 1995.

Willis, H.F., "Underwater Explosions, Time Interval Between Successive Explosions," British Report WA-47-21, 1941.

INITIAL DISTRIBUTION LIST

	No. Copies
1. Defense Technical Information Center 8725 John J. Kingman Rd., STE 0944 Ft. Belvoir, VA 22060-6218	2
2. Dudley Knox Library Naval Postgraduate School 411 Dyer Rd. Monterey, CA 93943-5101	2
3. Professor Young S. Shin, Code ME/sg Department of Mechanical Engineering Naval Postgraduate School Monterey, CA 93943	5
4. LCDR James E. Chisum 405 Beall Lane Central Point, OR 97502	2
5. Professor Anthony Healey, Code ME/he Department of Mechanical Engineering Naval Postgraduate School Monterey, CA 93943	1
6. Associate Professor Young W. Kwon, Code ME/kw Department of Mechanical Engineering Naval Postgraduate School Monterey, CA 93943	1
7. Associate Professor Steven R. Baker, Code PH/ba Department of Physics Naval Postgraduate School Monterey, CA 93943	1
8. Associate Professor Clyde Scandrett, Code MA/sd Department of Physics Naval Postgraduate School Monterey, CA 93943	1